Clonal hematopoiesis driven by chromosome 1q/MDM4 trisomy defines a canonical route toward leukemia in Fanconi anemia

Marie Sebert, Stéphanie Gachet, Thierry Leblanc, Alix Rousseau, Olivier Bluteau, Rathana Kim, Raouf Ben Abdelali, Flore Sicre de Fontbrune, Loïc Maillard, Carèle Fedronie, et al.

Version of Record: https://www.sciencedirect.com/science/article/pii/S1934590923000061
Manuscript_967ef6934f4913a36fc3100c594b26c8

Clonal hematopoiesis driven by chromosome 1q/*MDM4* trisomy defines a canonical route towards leukemia in Fanconi anemia

Marie Sebert[1,2,3,*], Stéphanie Gachet[1,3,4,*], Thierry Leblanc[5,6,#], Alix Rousseau[1,#], Olivier Bluteau[1,3,#], Rathana Kim[1,3,4], Raouf Ben Abdelali[1,3,4], Flore Sicre de Fontbrune[2,6], Loïc Maillard[1,3], Carèle Fedronie[1,3], Valentine Murigneux[7], Léa Bellenger[8], Naira Naouar[8], Samuel Quentin[1,3,4], Lucie Hernandez[1,3], Nadia Vasquez[1,3,4], Mélanie Da Costa[1,3,4], Pedro H. Prata[1,3], Lise Larcher[1,3,4], Marie de Tersant[1,3], Matthieu Duchmann[1,3], Anna Raimbault[1,3,4], Franck Trimoreau[4,9], Odile Fenneteau[10], Wendy Cuccuini[1,3,4], Nathalie Gachard[4,9], Nathalie Auger[11], Giulia Tueur[1,3,4], Maud Blanluet[12], Claude Gazin[3,13], Michèle Souyri[1,14], Francina Langa Vives[15], Aaron Mendez-Bermudez[16], Hélène Lapillonne[17], Etienne Lengline[2], Emmanuel Raffoux[2], Pierre Fenaux[1,2,3], Lionel Adès[1,2,3], Edouard Forcade[18], Charlotte Jubert[18], Carine Domenech[19], Marion Strullu[5,6], Bénédicte Bruno[20], Nimrod Buchbinder[21], Caroline Thomas[22], Arnaud Petit[23], Guy Leverger[23], Gérard Michel[24], Marina Cavazzana[25], Eliane Gluckman[2,26], Yves Bertrand[19], Nicolas Boissel[1,2,6], André Baruchel[1,5,6], Jean-Hugues Dalle[1,5,6], Emmanuelle Clappier[1,3,4], Eric Gilson[16], Ludovic Deriano[7], Sylvie Chevret[1,27], François Sigaux[1,3,4], Gérard Socié[1,2,28,31], Dominique Stoppa-Lyonnet[12], Hugues de Thé[1,3,4,30], Christophe Antoniewski[8], Dominique Bluteau[1,3,29,§], Régis Peffault de Latour[1,2,6] and Jean Soulier[1,3,4,§]

[1]Institut de Recherche Saint-Louis (IRSL), Université Paris Cité, 75010 Paris, France; [2]Clinical Hematology Departments, Saint-Louis Hospital, Assistance Publique-Hôpitaux de Paris (APHP), Paris, France; [3]INSERM U944/CNRS UMR7212, Paris, France; [4]Saint-Louis Hospital, Hematology Laboratory, APHP, Paris, France; [5]Robert Debré Hospital, Department

of Pediatric Hematology, Paris, France; [6]EA 3518, IRSL, Paris, France; [7]Genome Integrity, Immunity and Cancer Unit, INSERM U1223, Equipe Labellisée Ligue Contre Le Cancer, Institut Pasteur, Paris, France; [8]Sorbonne Université, CNRS FR3631, Inserm US037, Institut de Biologie Paris Seine (IBPS), ARTbio Bioinformatics Analysis Facility, Institut Français de Bioinformatique (IFB), Paris, France; [9]Hematology laboratory, CHU Limoges, Limoges, France; [10]Hematology Laboratory, Robert Debré Hospital, Paris, France; [11]Département de Biologie et Pathologie Médicales, Institut de Cancérologie Gustave Roussy, Villejuif, France; [12]Department of Genetics, Institut Curie, Université de Paris, Inserm U830, Paris, France; [13]Centre National de Recherche en Génomique Humaine (CNRGH), Institut de Biologie François Jacob, CEA, Evry, France; [14]INSERM UMR_S1131, Hôpital Saint Louis, Paris, France ; [15]Mouse Genetics Engineering Center, Pasteur Institute, Paris, France. [16]Université Côte d'Azur, Nice, France CNRS, Inserm, Institute for Research on Cancer and Aging, Nice (IRCAN), France, and Department of Medical Genetics, CHU, Nice, France; [17]Hematology Laboratory, Trousseau Hospital and HUEP, Paris, France; [18]CHU Bordeaux, Service d'hématologie et thérapie cellulaire et Unité d'Hématologie Oncologie Pédiatrique, F-33000 Bordeaux, France; [19]Institut of Hematology and Pediatric Oncology (IHOP), Université Lyon 1, Hospices Civils de Lyon, France, and Centre de Recherche en Cancérologie de Lyon, INSERM U1052, CNRS 5286, Centre Léon Bérard; Université Lyon 1, Lyon, France; [20]CHU de Lille, Pediatrics Hematology, France; [21]Centre pédiatrique de transplantation de cellules souches hématopoïétiques, CHU de Rouen, France; [22]Service d'oncologie-hématologie et immunologie pédiatrique, CHU de Nantes, France; [23]Pediatric Hematology-Oncology, Trousseau Hospital and HUEP, Paris, France; [24]Timone Enfants Hospital, Department of Pediatric Hematology and Oncology, and Aix-Marseille University, EA 3279, Marseille, France; [25]Biotherapy Department, Necker Children's hospital, APHP Centre; Biotherapy Clinical Investigation Center, Inserm U1416; and University of Paris, Imagine Institute, Paris, France; [26]Eurocord, Department of Hematology, Saint-Louis Hospital, Paris, France; [27]Division of Biostatistics, Saint-Louis Hospital, APHP, Paris, France; [28]INSERM UMR-976, Saint-Louis Hospital Paris, France; [29]EPHE, PSL University, Paris, France ; [30]Collège de

France, Paris, France; Centre de Référence Maladies Rares “Aplasie Médullaire”, Saint-Louis and Robert Debré hospitals, Paris, France.

Present address of D.B., CNRS UMR9019, Paris Saclay University, Gustave Roussy Cancer Campus, Villejuif, France

Lead contact :

Prof. Jean Soulier, MD-PhD
Saint-Louis Hospital
U944 INSERM Bat. Jean Bernard
1 Av. Claude Vellefaux, 75010 Paris, France
jean.soulier@aphp.fr
Phone: +33 1 53 72 40 32

[§]Dominique Bluteau and Jean Soulier are corresponding authors

[*]Marie Sébert and Stéphanie Gachet contributed equally

[#]Thierry Leblanc, Alix Rousseau and Olivier Bluteau contributed equally

Word counts: Abstract 150, text 4002.

Figures, 7; Tables, 0

Supplemental information: Supplemental Figures, 8; Supplemental Tables, 8.

SUMMARY

Fanconi anemia (FA) patients experience chromosome instability, yielding hematopoietic stem/progenitor cell (HSPC) exhaustion and predisposition to poor-prognosis myeloid leukemia. Based on a longitudinal cohort of 335 patients, we performed clinical, genomic and functional studies in 62 patients with clonal evolution. We found a unique pattern of somatic structural variants and mutations that shares features of BRCA-related cancers, the FA-hallmark being unbalanced, microhomology-mediated translocations driving copy-number alterations. Half the patients developed chromosome 1q gain, driving clonal hematopoiesis through *MDM4* trisomy downmodulating p53 signaling, later followed by secondary-AML genomic alterations. Functionally, *MDM4* triplication conferred greater fitness to murine and human primary FA HSPCs, rescued inflammation-mediated bone marrow failure and drove clonal dominance in FA mouse models. Targeting MDM4 impaired leukemia cells *in vitro* and *in vivo*. Our results identify a linear route towards secondary leukemogenesis whereby early MDM4-driven downregulation of basal p53 activation plays a pivotal role, opening monitoring and therapeutic prospects.

INTRODUCTION

Fanconi anemia (FA) is an inherited DNA instability disorder caused by biallelic mutations in one of the 22 *FANC* genes of the FA pathway, a network involved in DNA damage repair and stress response[1]. FA patient cells present with high levels of chromosome breaks induced by DNA interstrand crosslinkers (ICL), such as cisplatin or endogenous aldehydes. The upstream 'FA core' multiprotein complex activates the D2/I heterodimer, which functionally interacts with downstream proteins including BRCA2 (also known as FANCD1), resulting in replication-coupled excision of the ICL that is completed by homologous recombination (HR)[1]. FA patients can display various congenital malformations and frequently have a short stature[2]. Most of them experience progressive bone marrow (BM) failure (BMF) during childhood, the diagnosis of FA being often made at this stage, and many receive hematopoietic stem cell transplantation (HSCT)[2,3]. Later on, during their teens or young adulthood, the risk of myelodysplastic syndrome (MDS) and acute myeloid leukemia (AML) becomes high[4,5]. Still later, in adult patients, a range of solid cancers can be seen, especially squamous cell mouth cancer[6]. The rare FA patients with a biallelic BRCA2/FANCD1 mutated genotype exhibit an extreme predisposition to early onset MDS/AML and solid cancers[7]. While a rare disease, FA is nevertheless the most frequent inherited cause of BMF, and MDS/AML secondary to FA have a dismal prognosis in this frail population with a high chemotherapy-related toxicity[4,8,9].

We and others have clarified mechanisms underlying BMF and demonstrated the role of an exacerbated basal p53 signaling triggered by unrepaired DNA damage in FA progenitor cells[10–13]. However, how BM cells progress to myeloid malignancies in a background of cell-intrinsic genomic instability, chronic inflammation and stem

cell exhaustion is still poorly understood[4,14,15]. Given that secondary MDS and AML (sAML) develop with a high penetrance, the clinical practice is to monitor FA patients over time by BM morphological exam and karyotype. This provides the unique opportunity to examine BM cells longitudinally and to investigate the full path of step-wise progression events towards MDS and AML, including at early stages. With the aim of clarifying leukemogenesis in FA, we studied our cohort representing virtually all FA patients seen in France over a 18-year period, one-third of them having developed BM clonal evolution.

RESULTS

Bone marrow clonal evolution in FA patients

We studied a cohort of 335 FA patients from 300 unrelated families, with a median follow-up of 7.6 years (interquartile range, IQR, 2.9 to 12.1), at a median age at the last follow-up of 15.1 years (IQR, 9.8 to 23.7) (**Figure S1**). Relevant patient characteristics, including FANC genotype and hematological staging, are shown in **Table S1.** A total of 322 patients (96.1%) presented BMF, with a median age of 6.8 years (IQR, 3.7 to 10.2) at the first hematological signs, and 197 (58.8%) received HSCT at a median age of 10.5 years (IQR, 7.5 to 14.6). **Figures 1A** and **S2** shows clinical features according to patient age: at the age of 20, 88.3% (95%CI, 84.3 to 91.4) of patients had presented a BMF, of whom 61.2% (95%CI, 55.0 to 66.7) had undergone a HSCT. *Clonal evolution* was defined by the presence of cytogenetic abnormalities on BM karyotype, cytological evolution toward MDS (BM dysplasia with or without excess of blast, see the Methods section) or AML. Overall, 98 out the 335 patients (29.2%) experienced clonal evolution that was first seen at a median age of 13.8 years (IQR, 8.1 to 20.8; range 0.8 to 56 years) and included 51 patients (15.2%)

with blastic evolution (defined by more than 5% of BM blasts), seen at a median age of 16.0 years (IQR, 8.7 to 22.9; range 0.8 to 62 years) (**Figure 1A**). Four patients with the *BRCA2/FANCD1* genotype presented with an early blastic evolution (median age, 3.5 years), as previously described in this genotype[7]. The cumulative incidence of clonal evolution and blastic progression by the age of 40 years was 37% and 21.5%, respectively (**Figure 1A**). Importantly, of the 130 patients (38.8% of 335) who received HSCT for severe aplastic anemia without clonal evolution, none subsequently developed MDS or AML. Median overall survival (OS) in the entire cohort was 33.5 years (95% CI, 30.4 to 37.5) with 68.6% (95%CI, 62.7 to 74.9) patients alive by age of 20, and 33.3% (95%CI, 24.7 to 45.0) at age of 40 (**Figure 1B**). OS was significantly shortened by clonal evolution (HR=1.53, 95%CI, 1.10-2.1; **Figure 1C**).

Chromosomal rearrangements with recurrent copy-number abnormalities rather than point mutations yield clonal evolution in FA patients

For 62 patients with clonal evolution, we obtained one or more BM and/or blood cell samples and extensively studied the clonal cells and their paired non-hematopoietic cells (i.e. cultured skin fibroblasts). Together with a careful review of the BM diagnosis and staging of MDS and AML (**Table S2**), we sequenced a set of AML/MDS-associated genes and performed array-comparative genomic hybridization (aCGH), unbiased whole exome sequencing (WES), whole genome sequencing (WGS), and RNA-seq at various stages of BM FA progression (**Figure S1**, **Tables S3-S6, and Star*Methods**).

Overall, the most salient somatic lesions were unbalanced translocations leading to partial or complete copy number abnormalities (CNAs) of chromosomal

arms (**Figure 2**). FA patient samples exhibited more gross CNAs than sporadic (non-FA) AML cases taken as control (age-matched selected cases from the WES-based 'Beat-AML' program cohort study[16]). In contrast, FA patient samples did not display more point mutations than control AMLs (**Figure 2A**, and **Table S5**). Similar results on CNA and point mutation numbers were found when we compared FA AML data to the non-FA, pediatric AML dataset from the TARGET cohort[17] (the WGS discovery files from the TARGET; see **Star*Methods**) (**Figure S3**). Moreover, these recurrent CNAs due to unbalanced translocations significantly accumulated together with BM progression in the 62 clonal cases, suggesting that they may be involved in transformation in FA BM (**Figure 2B**). Remarkably, the CNAs most frequently involved the long arm of chromosome 1 with various partner chromosomes, leading to complete or partial 1q gain (1q+) in 32 out of 62 patients with clonal evolution (51.6%) (**Figure 2C**). A common duplicated region of 13.2 Mb was delineated at 1q32 that includes the *MDM4* (*MDM4 regulator of p53*) gene (**Figure 2C**). Other recurrent chromosomal translocations yielded partial gain of chromosome 3 long arm (3q+, 40.3%, duplicating the *MECOM-EVI1* oncogene[15]), partial loss of 7q or monosomy 7 (-7/7q-, 30.6%), lesions at 21q22 altering the *RUNX1* locus (*RUNX1*, 22.6%), and, less frequently, del(20q), del(11q), del(5q) and trisomy 8 (**Figures 2C** and **2D**). Gene fusions were rarely detected (five patients), only the *PRDM16-RUNX1* fusion being recurrent (**Figure 2D**, fusion partners are indicated in the legend).

We then analyzed the pathogenic point mutations and found that the *RUNX1* gene was the most frequently mutated gene (in 9 of the 62 cases, 14.5%), resulting in *RUNX1* alteration by mutation, deletion or gene fusion in 33.9% of the 62 patients (**Figure 2D**). Eleven out of 62 patients (17.8%) had a signaling gene mutation, such as in *NRAS* or *KRAS*, and these patients presented with an excess of blasts, either

as AML or MDS-EB (MDS with excess blasts). Somewhat less than expected for secondary MDS or AML with frequent complex karyotype[18–20], the *TP53* gene was deleted or mutated in only five patients (8.0%, a single one having biallelic lesions) (**Figures 2C** and **2D**). Finally, while the clonal cell fraction based on CNAs was >50% in all MDS/AML cases, unbiased WES and WGS did not identify any additional new gene that would be recurrently mutated with a VAF threshold of 10%.

A unique FA-associated genomic instability somatic pattern

We further examined, using WGS, the overall *mutational signatures*, i.e. the overall patterns of substitutions, indels and rearrangements (structural variants, SVs) that can be seen in the genome of FA AML[21–24]. We selected cases according to their underlying genotype, either FA core (upstream genes in the FA pathway, mainly *FANCA* as per the frequency in FA patients) or BRCA2 (the downstream, highly cancer-prone *BRCA2/FANCD1* gene), and compared data of these two FA groups with those of the non-FA, pediatric AML TARGET dataset[17].

The overall tumor mutational burden (TMB) in the FA AMLs was not different from the non-FA AMLs (**Figure 3A**). However, in addition to a common age-related signature (single-base substitution (SBS)1 and SBS5 signatures), the BRCA2 cases and – to a lesser extent – the FA core cases, displayed a BRCA-associated, SBS3 signature (**Figures 3B** and **S4A-C**). This *Breast, ovarian and pancreatic cancer signature*, previously identified in BRCA1 or BRCA2 mutated solid cancers and also known as *Homologous recombination deficiency* (HRD) signature[22,23,25], was virtually absent in non-FA AML patients (**Figures 3B** and **S4A-C**). Regarding the SVs, we found a salient rearrangement pattern in both the FA core and BRCA2 AML cases. These included large (>1 Mb) SVs, largely due to unbalanced chromosomal

translocations resulting in CNAs, but also an accumulation of intermediate-size (10-250 Kb) deletions (**Figures 3C, 3D,** and **S4D,E**; **Table S6**). We applied the HRDetect model to predict the 'BRCAness' based on mutation and SV pattern[21,25,26]. We found a high HRDetect score in the BRCA2 AMLs, as expected, but also – to a lesser extent – in the FA core AMLs compared to the controls, including an increased frequency of small deletions with microhomology (**Figure 3E**). In conclusion, FA MDS/AML cells harbor a unique FA-associated pattern of somatic variations that shares some features with the HRD signature of BRCA-related solid cancers, the hallmark of FA being unbalanced translocations yielding gross chromosomal CNAs.

FA 1q translocations frequently involve a fragile pericentromeric region and microhomology-mediated end joining DNA repair mechanism

To get mechanistic insights into the prominent unbalanced translocations found in FA clonal evolution, we used WGS-based paired-end analysis combined with karyotype and CNA information to sequence the translocation breakpoints (**Figure 3F**). This enabled us to analyze 33 translocation breakpoints from 10 AML cases and to infer the repair mechanism that generated them[27]. The breakpoint regions frequently display short stretches of DNA homology, reflecting prominent microhomology-mediated end joining (MM-EJ; also known as alternative non-homologous end joining repair, Alt-EJ)[27,28] as the preferential post-replicative repair mechanism in the FA context (**Figure 3F and Table S7**).

We then mapped all unbalanced chromosomal translocation breakpoints using the CNA data from the 62 patients with clonal evolution. Strikingly, the proximal breakpoints at chromosome 1q focused at the centromeric/pericentromeric repeated region in 25 out of 32 1q+ cases (78.1%, **Figure 3G**); by contrast the proximal

breakpoints spread along the chromosome arms in the other unbalanced translocations such as in 3q+. Remarkably, historical cytogenetic studies of FA cells have shown increased rate of chromosome breaks at the 1q12 pericentromeric region, also known as fragile site FRA1J[29,30]. We found spontaneous breaks in this region in FA blood cells (**Figure 3H**), and it was also involved in clonal 1q+ translocations in FA MDS/AML, as demonstrated by fluorescence in situ hybridization (FISH) (**Figure 3I**). Finally, breakpoint sequence analysis revealed Satellite II and III sequences, characteristic of pericentromeric heterochromatin[31], but not centromeric sequences, at these proximal 1q+ breakpoints (**Figure 3F** and **Table S7)**.

Collectively the data suggest that the large pericentromeric heterochromatin region at 1q12 is a recurrent fragile site of spontaneous breaks in FA cells, the abnormal repair of which by MM-EJ eventually results in unbalanced translocations yielding 1q copy gain.

1q duplication triggers increased expression of *MDM4*, a negative modulator of p53 activity

We then aimed to elucidate which potential cancer drivers may be triggered by 1q+, the most frequent somatic lesion in FA MDS/AML. Remarkably, the 13.2 Mb common duplicated region at 1q32 included the *MDM4* oncogene, located just beside (40 Kb) the telomeric border (**Figure S5A**). *MDM4* (also known as *MDMX* or *HDMX*) is a negative regulator of p53 activity that can be amplified or overexpressed in mouse and human cancers including MDS and AML[32–35]. We previously demonstrated that the constitutive activation of the p53 pathway in FA BM yields loss of hematopoietic stem and progenitor cells (HSPCs)[10]. Therefore, we hypothesized that 1q duplication may attenuate the FA-associated p53 pathway hyperactivation through increased

gene dosage of *MDM4*. We first analyzed by RNA-seq CD14+ cells from 56 FA patients before or after clonal progression, along with nine healthy (non-FA) controls (see **Star*Methods**, **Figure S5B,** and **Table S8)**. We found that the expression of many 1q genes was increased, consistent with a gene dosage effect, in 1q+ *versus* non-1q FA samples (**Figures S5A and S5C**). Specifically, *MDM4* gene expression was significantly increased in 1q+ cells, at the expected range for 3 *MDM4* copies instead of 2, whereas *MDM2* – not located in chromosome 1q – expression was not (**Figure 4A**). Gene set enrichment analysis (GSEA) showed an overall p53 pathway activation in the FA cells before clonal evolution when compared to healthy controls (**Figure 4B**, left panel), as predicted from our previous studies[10]. Once clonal, FA cells bearing a 1q+ displayed an attenuated p53 pathway profile when compared to clonal, but non-1q, cells from other FA patients (**Figure 4B**, right panel). Consistently, a MDM4-associated gene set, derived from *Mdm4* knock-out fetal liver, was enriched in the 1q+ *versus* non-1q clonal cells (**Figure S5D**). Downregulated expression of some major p53 response genes in 1q+ FA cells was found at the RNA and at the protein level when compared to pre-clonal stages (**Figure 4C** and **Figure S5E**). These data, derived from primary patient cells, strongly support our proposal that a gene dosage-dependent upregulation of *MDM4*, related to 1q+, attenuates the exacerbated p53 pathway in FA cells and acts as the master regulator switch of clonal expansion.

1q+/*MDM4* confers a growth advantage to human and mouse FA HSPCs and rescues bone marrow failure induced by chronic inflammatory stress

HSPCs growth capacities are deficient in FA upon DNA damage accumulation and can be rescued by attenuation of the p53 response[10,11]. When evaluated *in vitro* by

methylcellulose colony-forming unit granulocyte/macrophages (CFU-GM) assays, primary 1q+ FA patient progenitor cells recovered CFU-GM capacity, contrasting with those from non-1q FA patients (**Figure 4D**). We then used BM Lin$^-$ cells from *Fancg*$^{-/-}$ mice to evaluate functionally the effect of increased *Mdm4* expression on FA progenitor cells. Lentiviral transduction of *Mdm4* rescued clonogenicity at the same level as *Trp53* knockdown (**Figure 4E** and **Figure S6A**). Importantly, similar data were obtained when we overexpressed *MDM4* in primary BM CD34+ cells from FA patients (**Figure 4F**).

We next sought to check the effect of *MDM4* trisomy *in vivo,* using a model in which this gene would be expressed upon its endogenous regulatory regions in FA HSPCs, thus mimicking the patient setting. To this end, we engineered a *Mdm4* duplicated transgenic (*Mdm4*^{Tg}) mouse strain by inserting the full *Mdm4* genomic locus using a Bacterial Artificial Chromosome (BAC) encompassing *Mdm4* and flanking regions, which resulted in mild *Mdm4* overexpression due to gene dosage (**Figure 4G** and **Figure S6B)**. We then silenced *Fancd2* in BM Lin$^-$ cells from both wildtype and *Mdm4*^{Tg} mice (**Figure S6C,D**) and co-injected those FA-like cells in competition in recipient mice. Remarkably, although only implanted at 10% of the inoculate, *Mdm4*^{Tg} FA-1q+-like cells overcame the control FA-like cells, demonstrating their competitive advantage *in vivo* (**Figure 4H** and additional experiment **Figure S6E-G**).

Fanc-deficient mice do not develop an overt bone marrow failure (BMF) unless exposed to chronic stress such as inflammation or aldehydes[11,13]. Therefore, we crossed *Fancg*$^{-/-}$ and *Mdm4*^{Tg} mice and challenged *Fancg*$^{-/-}$, *Fancg*$^{-/-}$*Mdm4*^{Tg}, and control mice with serial pI:pC injection (**Figure 4I**). Strikingly, the resulting BMF of *Fancg*$^{-/-}$ mice was not observed in the *Fancg*$^{-/-}$*Mdm4*^{Tg} mice, experimentally

demonstrating the impact of the genetic duplication of the *Mdm4* locus to rescue *Fancg*$^{-/-}$ hematopoiesis under stress.

MDM4 inhibition impairs 1q+ FA AML cells

To investigate the effect of MDM4 inhibition in 1q+ FA cells, we silenced *MDM4* in FA-AML1, a cell line established from a FA patient with 1q+ AML. We found greater p53 and p21 protein levels, together with increased apoptosis and decreased S-phase, demonstrating that in these cells, p53 signaling is under tight MDM4 control (**Figure 5A-C**). We also exposed the FA AML cells to SJ-172250, a small molecule inhibitor of MDM4, and found that cell growth, clonogenicity and S phase were impaired, and apoptosis induced, in contrast to *TP53*-mutated, non-FA AML cells (**Figure 5D-F**).

Recently, MDM4 inhibitors have been developed for therapeutic purposes, ALRN-6924 being a clinical-grade, p53 stapled peptide MDM4/MDM2 inhibitor proposed as a therapeutic strategy in AML[32]. We found that ALRN-6924 impaired the growth, clonogenicity and S phase in the FA-AML1 cells (**Figure 5G-I**). Importantly, clonogenicity of primary 1q+, but not non-1q, AML cells from FA patients was significantly decreased upon ALRN-6924 exposure (**Figure 5J**).

To test ALRN-6924 *in vivo*, we performed xenograft experiments using FA-AML1 cells injected in immunodeficient NOG-EXL mice. ALRN-6924 treatment of established xenografted tumor cells resulted in a significant reduction of leukemic burden *in vivo*, suggesting potential therapeutic use in FA patients with 1q+ MDS/AML (**Figure 5K**). However, because p53 activation in the residual FA cells may accelerate BMF[10], such treatment would have to be used with the support of (non-FA) healthy HSPCs, i.e. in combination with HSCT.

A canonical model in which 1q+/MDM4 triggers preleukemic, clonal hematopoiesis

To integrate the timing and role of 1q+/*MDM4* in the overall dynamic of clonal hematopoiesis and AML development in FA (**Figure 6A**), we longitudinally studied those patients with an isolated 1q+ and available serial BM samples (**Figure 6B**). None of these patients had an excess of BM blasts at first 1q+ detection. Five (5/15) did not experience further clonal evolution with a median follow up of 3 years (range 1-7 years; one received HSCT after 2 years history of BMF). The ten others acquired additional driving events with a median time to acquisition of 3 years (range, 1-8); of those, 4 had blastic progression (>5% BM blast cells; median time to blast >5%, 3.25 years) (**Figure 6B**).

We then ranked the oncogenic events with respect to BM progression in the patients, using the global Bradley and Terry model (**Figure 6C**). Remarkably, 1q+/MDM4 occurred early, i.e. before blastic evolution, whereas 3q+/EVI1, -7/del7q, and *RUNX1* alterations occurred later, *RUNX1* alterations being the latest events. Moreover, the combined analysis of aCGH CNA ratios, NGS variant allele frequency (VAF), karyotype formula and FISH on longitudinal samples enabled us to determine the architecture of stepwise clonal evolution in FA BM. Clonal evolution was not branched, but linear, in all informative cases, without clone sweeping (a new, distinct clone that would expand and overcome the former 1q+ clone) (**Figure 7**). We analyzed gene expression according to BM stage in the FA samples using RNA-seq data. While p53 pathway was activated at the early (non-clonal) stage, this was subsequently attenuated after transition to 1q+ clonal hematopoiesis, but not in patients with non-1q clonal evolution (**Figure 6D**). We further analyzed paired BM

samples from the same patient (N=5 patients), before and after trisomy 1q acquisition, finding consistent data using a set of p53 response genes (**Figure 6E**).

Collectively, our data points to a canonical, step-wise, linear, 1q+/MDM4 tumor progression route in FA bone marrow, as summarized in **Figure 6F**. Importantly, in these patients, 1q/MDM4 trisomy drives early clonal hematopoiesis rather than *bona fide* blastic transformation, the latter only occurring along with linear acquisition of additional driver events such as 3q+/*MECOM-EVI1*, 7q-, *RUNX1* inactivation, or signal transduction activation (**Figures 2D** and **6B,C**).

We analyzed longitudinal blood cell counts (BCC) in patients who experienced an isolated 1q+ clonal hematopoiesis (**Figure S7**). While BCC values did not clearly improve at 1q+ first karyotype detection, they remained stable over years, as subnormal or moderately cytopenic, at ages at which other FA patients usually experience severe cytopenias and HSCT. Accordingly, while the median age at HSCT for severe BMF in the FA cohort was 10.5 years (N=197 patients), the median age of HSCT in FA patients with 1q+ (performed essentially for MDS/AML) was 15.2 years (N=27), suggesting that 1q+ clonal hematopoiesis may, at least partially, compensate for severe BMF.

DISCUSSION

The sustained p53 response seen in FA HSPCs acts as a potent anti-cancer barrier upon intrinsic FA-driven genomic instability but contributes to BMF[10]. We discovered that 1q trisomy is the most frequent and early event in the natural history of BM evolution in FA, driving enforced *MDM4* oncogene expression through gene dosage and repressing high basal p53 response. Such p53 attenuation confers a keen advantage to 1q+ cells over bystander FA cells, triggering stem/progenitor cell

survival and clonal expansion of phenotypically normal 1q+ cells as we demonstrated experimentally *in vitro* and *in vivo*. Our thorough analysis of the individual BM natural histories demonstrates that 1q+ is not transforming *per se*, and that cells with 1q+ represent a preleukemic population resembling clonal hematopoiesis of indeterminate potential (CHIP) or clonal mosaicism with chromosome alterations[36–40]. In this respect, 1q+ clones readily expand and repopulate the exhausted bone marrow, and subsequent transition towards MDS/AML correlates with linear acquisition of additional oncogenic lesions.

It is noteworthy that MDS and AML in humans can develop *de novo* or secondary to pre-existing hematologic disorders such as in inherited BMF (including FA), myeloproliferative neoplasms, MDS or exposure to chemotherapy[41–45]. Although secondary leukemias represent a highly heterogeneous group, they frequently share features that include BM dysplasia, complex karyotype with del(7q) and frequent *TP53* gene inactivation. Our longitudinal analysis in FA, a DNA damage repair disorder, draws a model oncogenic route of sAML which illuminates the pivotal role of p53 pathway modulation in preleukemic clonal hematopoiesis in the context of intrinsically stressed hematopoiesis[38,42–44]. In contrast, FA cells did not display mutations of key epigenetic regulators driving CHIP, i.e. *TET2* or *DNMT3A*, nor splice or cohesin gene mutations as seen in non-FA MDS or AML, highlighting distinct initiation mechanisms of disease in *de novo* and secondary leukemia. It is noteworthy that we did not observe leukemia in *Fancg*$^{-/-}$*Mdm4*^{Tg} mice after 64 weeks of follow up under chronic inflammatory stress, showing that we modeled clonal hematopoiesis rather than overt AML.

We further uncovered a unique overall somatic pattern of structural and mutational variants in FA AML cells, which features frequent MM-EJ mediated

rearrangements rather than point mutations. These rearrangements includes unbalanced translocations leading to complete or partial chromosome arm gains and losses, and a pattern of genomic deletions which resembles BRCA-associated HRD genomic instability, rather than an 'hypermutator' substitution phenotype as in other DNA integrity deficient disorders like xeroderma pigmentosum[46]. These features in FA AML are consistent with previous observations in FA cell lines and mice[11,47–49]. Interestingly, this unique FA-associated, somatic pattern of structural and mutational variants in FA AML informs on how the FA pathway protects the HSPC genome. Overall, the FA-intrinsic chromosomal instability and the fragile site at the 1q pericentromeric heterochromatin region, combined to the relative "hypomutability" of FA cells[47–49], are plausible reasons for which 1q/*MDM4* translocations may occur frequently, as a "surrogate" of *TP53* mutations, conferring in one single event an immediate advantage to FA HSCs which are upon strong p53 pressure[10]. In the context of FA in which fragile sites are stressed[29,30,50,51], spontaneous breaks at this site and subsequent MM- or NHEJ-mediated repair result in 1q+ and *MDM4*-driven p53 signaling attenuation. Cells can then expand as clonal hematopoiesis but their genomic instability licenses the onset of additional structural aneuploid rearrangements[52], see a mechanistic model in **Figure S8**.

Our clinical study demonstrates that clonal evolution in FA is associated with a shorter overall survival. Beside the FA patients who benefited from early HSCT for severe BMF (38.8%), the remaining population is at risk of clonal evolution, 1q+ being the first event. Currently, isolated 1q+ is not *per se* a formal HSCT criteria and the years of event-free survival in FA patients with isolated 1q+ represents an opportunity of careful watch-and-wait policy, along with HSCT preparation. Interestingly, longitudinal blood cell count data in the patients suggest that 1q+

HSPCs may support some subnormal hematopoiesis, in line with our functional experiments in mice. In contrast, additional events like 3q+, del7q/-7 and *RUNX1* inactivation correlated with blastic evolution, prompting short term HSCT[9]. Based on our data, we recommend combining a CNA and mutation analysis to classical morphological and karyotype examination on longitudinal BM aspiration, in order to monitor BM staging and help in decision-making, particularly timely HSCT. This workup can be performed every year or less often, depending on the age, BM morphology and stability of the blood cell counts. CNA analysis can be performed using FISH on recurrent loci with a standard 5-10% cell threshold, or pangenome using aCGH, WES or WGS with a 10-20% VAF threshold depending on sequencing coverage. More sensitive detection of 1q+, 3q+ and 7q- CNA clones in the BM would need single cell DNA sequencing or sequencing after multiple colony sorting.

In this frail population where HSCT is currently the only option, new therapeutic approaches are needed. Our results suggest that MDM4 inhibitors[32] may have clinical activity in 1q+ MDS/AML FA patients, a proposal that may be tested in pragmatic patient studies in this rare disease. Moreover, the finding that FA AML cells display some HRD, BRCA-like signature features raises the prospect that poly(ADP ribose) polymerase (PARP) inhibitors may also have clinical benefit[53]. However, because patients are constitutively FA-deficient, targeted drugs such as MDM4 or PARP inhibitors may accelerate marrow failure and might have benefit only when used with the support of healthy hematopoietic cells, i.e. in combination with HSCT at the MDS-EB/AML stage or in post-transplant AML relapse[3,54], or in complement to gene therapy[54], the new healthy, non-FA HSCs or FA-corrected HSCs being insensitive to the inhibitors.

Limitations of the study

We modelled clonal hematopoiesis associated with 1q+ in FA mice, rather than overt leukemia. Future models may implement additional oncogenic events (*MECOM/EVI1* overexpression, *RUNX1* inactivation or *NRAS/KRAS* mutation) aimed at obtaining secondary FA-AML which could be further explored.

Although our studies establish the important functional role of *MDM4* triplication, it remains possible that one or several other genes on chromosome 1q may behave as co-driver of fitness, a phenomenon frequent in cancer aneuploidy[55].

Finally, while 1q+ is the most frequent event leading to clonal hematopoietic evolution in FA patients, a fraction of them developed AML without 1q+, paving the way to complementary studies exploring the underlying alternative leukemogenesis pathways.

ACKNOWLEDGMENTS

This study received support from the European Research Council (ERC) Consolidator Grant to J.S. (CEVAL-311660); the FP7 Eurofancolen program (HEALTH-F5-2012-305421); the ANR program PACRI (Projet alliance parisienne des instituts de recherche en cancérologie); the CONECT-AML (Collaborative Network for Children and Teenagers with Acute Myeloid Leukemia) program supported by a grant from the Institut National du Cancer (INCa), Fondation ARC, Ligue nationale contre le cancer, and Laurette Fugain (INCa-ARC-LIGUE_11905) to JS and CA ; and the Association Française pour la Maladie de Fanconi (AFMF) grants 'Histoire naturelle de la maladie de Fanconi' to RPL and JS, 'Modélisation de la transformation leucémique dans la maladie de Fanconi' to DB, and 'Cribles fonctionnels à haut débit

de gènes modificateurs de la maladie de Fanconi' to CG. M.S. was supported by the AVIESAN-INCa Program "Formation à la Recherche Translationnelle", and A.R. by a grant from the Fondation ARC. The work in E.G.'s lab is supported by Fondation ARC and ANR Telochrom. The work in L.D.'s lab is supported by INCa (PLBIO16-181) and ERC (310917).

Saint-Louis/Robert Debré Hospital is supported by the French Government (Direction de l'Hospitalisation et de l'Organisation des Soins) as the Centre de Référence Maladies Rares (CRMR) "Aplasies Médullaires Constitutionnelles", filière MARIH. The Institut de Recherche Saint-Louis (IRSL, Université Paris Cité) is supported by the ANR IHUB program as "THEMA, the French National Center for Precision Medicine in Leukemia".

We would like to especially thank the patients and their families, the Association Française de la Maladie de Fanconi (AFMF), and all physicians and nurses for taking care of the patients. We would also like to thank Véronique Parietti at the Animal Experimentation platform, and Niclas Setterblad and Antonio Alberdi at the Genomic Platform, Institut de Recherche Saint-Louis (IRSL), Paris, France. We also acknowledge the worldwide contributions from users and developers towards the Galaxy Project and the software ecosystem that we use and rely on.

AUTHOR CONTRIBUTIONS

J.S. conceived and led the project. M.S., S.G., T.L., O.B., R.B.A, F.S., C.A., D.B., R.P.L. and J.S. managed the project. M.S., S.G., A.Ro., O.B., R.K., R.B.A., L.M., C.F., L.H., L.L., P.H.P., M.dT., M.D., M.B., C.G., M.S., F.L.V., A.M.B., H.L., E.C., E.G., F.S., D.S.L., H.dT., D.B. and J.S. generated, processed and/or analyzed the experimental data. T.L., F.S.F., E.L., E.R., P.F., L.A., E.F., C.J., C.D., M.S., B.B.,

N.B., C.T., A.P., G.L., G.M., M.C., E.G., Y.B., N.B., A.B., J.H.D., G.S. and R.P.L. provided clinical data and samples. T.L., N.V., M.D.C., F.S.F., R.P.L. and J.S. coordinated sample acquisition. F.T., O.F. and A.Ri. performed morphological review. W.C., N.G., N.A. and G.T. performed cytogenetic analyses. V.M., L.B., N.N., S.Q., L.D., F.S. and C.A. performed bioinformatic analyses. M.S., S.G. and S.C. performed statistical analyses. M.S., S.G., C.A., and J.S. drafted the manuscript and figures. All authors approved the manuscript.

DECLARATION OF INTERESTS

J.S. is scientific advisor for STRM.BIO, Inc (Boston, USA).

The other authors declare no competing interest.

INCLUSION AND DIVERSITY FORM

One or more of the authors of this paper self-identifies as an underrepresented ethnic minority in their field of research or within their geographical location.

FIGURE TITLES AND LEGENDS

Figure 1. Hematologic natural history and outcomes in the French FA cohort.

(A) Cumulative incidence of bone marrow failure (BMF), HSCT, clonal evolution, MDS with excess of blast cells or AML (MDS-EB/AML), and solid cancer in the entire French FA cohort. Specifically, the curves report the cumulative probability of each event by the proportion of patients from the whole population of 335 patients who have developed the event of interest by that age. The numbers of patients exposed to the risk of each event over age are below the graph.

BMF, clonal evolution and MDS-EB/AML events were censored at HSCT, since patients who received HSCT were not further at risk of developing these specific events; therefore, patients who received HSCT were not included further in the number below the graph for these events. By contrast, the solid cancer curve was not censored at HSCT since transplanted patients are still exposed to that risk. Of note, patients with EB-MDS/AML are also included in the *clonal evolution* (as defined in the Result section) curve.

(B) Overall survival (OS) in the entire cohort, not censored at HSCT. The shaded area refers to the 95% confidence bands around the survival estimates.

(C) OS according to clonal evolution defining a time-dependent covariate (where clonal denotes the group of patients after clonal evolution, and non-clonal the group of patients before the time of clonal evolution and those who do not exhibit any clonal evolution), not censored at HSCT. Statistical analysis was performed using the Mantel-Byar test (see Method section).

See also **Figures S1** and **S2**.

Figure 2. Chromosomal rearrangements with recurrent copy number abnormalities (CNAs) are associated to clonal evolution in FA.

(A) Somatic abnormalities in AML cells as evaluated by WES in 13 'FA core' patients, compared with AMLs from 27 age-matched patients from the Beat-AML cohort as non-FA controls. Left panel, number of CNAs per case in FA patients (median number, 3 CNAs; range, 0-10), compared with non-FA AML controls (median number, 0 CNA; range, 0-4). Right panel, number of point mutations and insertions/deletions (indels) per case in FA patients (median number, 8 mutations; range, 5-15), compared with non-FA controls (median number, 10 mutations; range, 2-26). *P* values using the Wilcoxon test are indicated. FA-AML core patients with available material were randomly selected.

(B) Number of somatic lesions in 62 clonal FA patients as shown according to their stage of BM progression. Left panel, number of CNA per case (as detected by aCGH); right panel, number of substitutions and indels per case (as detected by gene panel). The indicated *p* values were calculated using an Anova test, the global significance being shown. Morphologically-defined BM stages were bone marrow failure (BMF, N=10); MDS multi-lineage dysplasia (but without excess of blast cells) (MDS-MLD, N=15); MDS with excess of blast cells (MDS-EB, N=12); acute myeloid leukemia (AML, N=25).

(C) Mapping of the CNAs from FA clonal BM cells. CNAs are shown according to their chromosomal position (vertical axis) and frequency (horizontal axis). Horizontal solid and dash lines delineate chromosome from short to long arm. Deletions and gains are shown on the left (blue) and right (orange), respectively, as the number of cases with CNA at each position /total number of clonal cases, showing the overall CNA frequency at each position. Therefore, the peaks delineate the (minimal)

common regions of gain or deletion. The four main recurrent gained or lost regions are indicated by an arrow; the arrow points the commonly gained (at chromosome 1q/*MDM4* and 3q/MECOM-*EVI1*) or deleted (at 7q and 21q/*RUNX1*) regions and the underlying oncogene or tumor suppressor gene.

(D) Recurrent somatic chromosomal and molecular abnormalities in the BM cells of 62 FA patients with clonal evolution. When multiple timepoints were available for the same patient, the latest data is shown (one column by patient). Upper panel, gains, losses, and translocations, as identified using karyotype, aCGH, myeloid next-generation sequencing (NGS) panel, WES, and/or RNA-seq analyses for fusions. CNAs and translocations were ordered by frequency, the values being shown on the right. Fusions were *PRDM16-RUNX1* (patients EGF036, EGF216, and EGF299), *PRDM16-ZFP36L2* (EGF037), and *RUNX1* with an unidentified partner (EGF111). The near-entire *PRDM16* gene at 1p36 was retained in the translocations; by contrast, *RUNX1* at 21q22 was interrupted and, when the 21q22-qter region was gained, *RUNX1* was never located in the gained part (not shown). Lower panel, pathogenic substitutions and indels, as identified using NGS myeloid cancer gene panel (**Table S4**) or WES (**Table S5**).

See also **Figure S1** and **S3**.

Figure 3. A unique FA-associated somatic pattern of structural variants and mutations that shares several features with BRCA-related cancers.

(A) Tumor mutational burden (TMB) in *FA core* (N=11), *BRCA2* (N=5) and non-FA pediatric (N=30 from the TARGET cohort) AMLs. Each dot represents an AML case.

(B) Mutational COSMIC signature usage; the BRCA-related SBS3 signature is shown

by an arrow; the other frequently represented signatures were SBS1 and SBS5 (aging), and SBS16 (unknown).

(C) Small/intermediate-size (1kb - 1Mb) structural variant (SV) distribution according to their size; deletions and duplications are shown, while inversions (not shown) were virtually absent. *P* values were obtained by t-test (**, $p < 0.01$); detailed values are shown in **Figure S4D**.

(D) Large (> 1Mb) SV distribution; deletions, duplications and neutral copy-number loss of heterozygosity (LOH) are shown; *p* values are shown in **Figure S4E**. Data were manually cured by case-by-case comparison with aCGH and, when available, WES data.

(E) HRDect score value and number of small deletions 5-60nt with microhomology in the three groups (left and right, respectively); *P* values were obtained by t-test (**, $p < 0.01$; ***, $p < 0.001$; ****, $p < 0.0001$).

(F) Microhomology-mediated end joining (MM-EJ, also known as Alt-EJ) repair as the prominent mechanism resulting in unbalanced translocations and clonal evolution in FA BM cells. A representative case with a duplication 1q is shown; the sequence of the breakpoint region harbored a short microhomology (*CC*) that enables to assign the repair pathway as MM-EJ in this case. Below are shown the inferred DNA repair pathways that generated unbalanced translocations in FA; NHEJ, non-homologous end joining; FoSTeS, fork stalling and template switching repair[27].

(G) Mapping of the proximal breakpoints from the unbalanced translocations in chromosome 1 and 3. Each breakpoint is represented by a star; the centromere and pericentromeric regions are highlighted in light blue.

(H) A FRA site at 1q21 pericentromeric region in FA hematopoietic cells. Representative spontaneous break at pericentromeric region in blood cells of a FA

patient at the BMF stage. This chromosomal location has been reported as a frequent spontaneous break location in FA cells[29]; this 1q pericentromic fragile site is also known as FRA1J.

(I) FISH analysis confirmed the involvement of the 1q12 pericentromeric region, rather than the centromere itself, in 1q+ clonal evolution of a representative FA patient, the green pericentromeric signal (RP11-326G211 BAC probe) being duplicated in the dup(1q), whereas the red centromeric signal (CENP-A) was not. Incidentally, the RP11-326G211 BAC conferred a small extra-signal at 1p11, as shown on the ideogram, which was not involved in the rearrangement. Left, normal chromosome; right, 1q duplicated chromosome.

See also **Figures S1** and **S4**.

Figure 4. 1q/*MDM4* trisomy confers a better fitness to FA HSPCs through p53 response attenuation.

(A) *MDM4* increased expression in CD14+, 1q+ *versus* non-1q, FA cells (one sample per patient, N=10 and 46, respectively, see Star*Methods and Figure S5B); *MDM2,* shown as a control, is non overexpressed. *, $p < 0.05$ using the Welch test, Benjamini-Hochberg corrected *p* values for multiple tests. The value of *MDM4* median expression in the 1q+ cases was within the 1% range of the expected value (5.35 *versus* 5.40, this last being inferred from a 1.5-fold increase from the non-1q value as per 2 to 3 alleles; note the log2(x+1) transformation y scale).

(B) P53 pathway enrichment analysis was scored using the GSEA algorithm (broadinstitute.org) in the non-clonal FA *versus* (non-FA) healthy samples, and in the 1q+ *versus* clonal non-1q (left and right plots, respectively). Of note, baseline

characteristics of 1q+ *versus* clonal non-1q patients matched closely (sex ratio, range of age, and stage of tumor progression with or without BM blast cells > 5%) and therefore cannot explain distinct GSEA profiles.

(C) Longitudinal immunoblot analysis of total BM cells before and after isolated 1q+, i.e. at the clonal hematopoiesis stage (2 patients, EGF168 and EGF289).

(D) CFU-GM assay on primary BM progenitor cells from healthy subjects, non-1q, and 1q+ FA patients (N=3, 13, and 7, respectively); for each, 10^4 primary CD34+ cells were plated and colonies were counted at day 7.

(E) CFU-GM assay on progenitor cells from *Fancg*$^{-/-}$ mice (N=9 mice). Murine *Mdm4* and *Trp53* were lentivirally overexpressed or silenced, respectively, in Lin$^-$ BM cells; 2x10^3 GFP+ cells were plated for each condition and colonies were counted at day 14. (F) CFU-GM assay on FA patient progenitor cells after *MDM4* transduction. Primary BM CD34+ cells from N=10 non-clonal FA patients were lentivirally transduced using human *MDM4*, *shTP53*, or controls; 10^3 cells were plated in each condition and colonies were counted at day 14. Note that tenfold fewer cells were plated in F than in D. For D-F, *p* values were obtained by the Mann-Whitney test; *, $p < 0.05$; **, $p < 0.01$; ***, $p < 0.001$; ****, $p < 0.0001$.

(G) *Mdm4* gene locus duplication and expression in *Mdm4*^{Tg} mice. Left, *Mdm4* locus genomic duplication, as assessed by aCGH in the *Mdm4*^{Tg} and WT lines; Right, Mdm4 protein expression in BM Lin$^-$ cells from *Mdm4*^{Tg} mice and controls. Normalized densitometric quantification demonstrated a significant 1.4-fold increase in *Mdm4*^{Tg} *versus* WT cells; individual mice ID and quantification values are shown; *, $p < 0.05$, using the Mann-Whitney test.

(H) Competitive transplant experiment. Top, BM Lin$^-$ cells from WT Ly5.1 and *Mdm4*^{Tg} mice, transduced with the short hairpin ribonucleic acid (shRNA) *Fancd2*

lentivector (LV), were injected into lethally irradiated wild type CD45.1 recipients. Engraftment kinetics was monitored monthly by BM sampling of recipient mice and flow cytometry analysis. O/N, overnight. Bottom**,** Engraftment kinetics of CD45.1 (WT*)* and CD45.2 (*Mdm4*^{Tg}) Lin^{-} cells injected in competition at a measured WT/*Mdm4*^{Tg} proportion of 91/9, after lentiviral *Fancd2* silencing (resulting in FA-like cells), comparing the percentages of CD45.1^{+} and CD45.2^{+} cells, respectively, in total BM at each timepoint. A low fraction of BM cells was CD45 negative, most of them being red blood cells, explaining why the later points did not add up to 100%. Each red (CD45.1^{+}) and blue (CD45.2^{+}) circle represents the median percentage in the total BM cells from 5 mice, the standard deviation being shown by vertical bars. For each time point, *p* values were obtained by the Mann-Whitney test; in addition, *p* value is shown for overall comparison of the two groups by Anova test; *, $p < 0.05$; **, $p < 0.01$; ****, $p < 0.0001$.

(I) Chronic stress-induced BMF experiment. Mice from the 4 genotypes (*Fancg*$^{-/-}$, n=7 mice; *Fancg*$^{-/-}$*Mdm4*^{Tg}, n=8; WT, n=5; and *Mdm4*^{Tg}, n=6) were exposed to 8 cycles of serial peritoneal injection of pI:pC during 4 weeks followed by a further 4-week recovery period (1 cycle). Peripheral white blood cell (WBC) counts of the mice are shown in the graph; *p* values were obtained by the Mann-Whitney test comparing *Fancg*$^{-/-}$*Mdm4*^{Tg} to *Fancg*$^{-/-}$ mice; *, $p < 0.05$; **, $p < 0.01$.

See also **Figure S1, S5** and **S6**.

Figure 5. *MDM4* silencing and treatment with MDM4 inhibitors of FA 1q+ AML cells.

(A) Immunoblot analysis of 1q+ FA-AML1 cell after MDM4 silencing using two specific shRNA (#56 and #59); ZsGreen-sorted cells were analyzed.

(B) and (C) Survival and cell cycle were analyzed on ZsGreen-gated, 1q+ FA-AML1 cells after MDM4 silencing. *P* values were obtained by t-test; *, $p < 0.05$; **, $p < 0.01$; ***, $p < 0.001$; statistical analysis for cell cycle compared phase S.

(D) Time-dependent changes in viability in the 1q+ cell line FA-AML1 *versus* the non-FA, *TP53*-mutated K562 cell line when treated with the MDM4 inhibitor SJ-172550 at 50µM (IC50); annexin-negative IP-negative cells are shown.

(E) Serial replating capacity, as measured by colony forming cell (CFC) assay, of FA-AML1 cells treated with increasing doses of SJ-172550.

(F) Cell cycle analysis in FA-AML1 and K562 cell lines after 24 hours of 50µM SJ-172550 treatment**;** statistical analysis compared phase S.

(G) Time-dependent changes in viability and apoptosis in FA-AML1 cells *versus* K562 cells after treatment with the MDM2/MDM4 dual inhibitor ALRN-6924 at 1.8µM (IC50). (H) CFC assay of FA-AML1 cells treated with increasing doses of ALRN-6924.

(I) Cell cycle analysis in FA-AML1 and K562 cell lines after 24 hours of ALRN-6924 treatment at 1.8 µM; statistical analysis compared phase S.

For (B) to (I), *p* values were obtained by t-test; *, $p < 0.05$; **, $p < 0.01$; ***, $p < 0.001$; ****, $p < 0.0001$; ns, non significant.

(J) CFU assay of primary 1q+ or non-1q CD34+ cells from FA patients with AML (N=7 each) upon exposure to 0.1 µM ALRN-6924; for each patient, 10^4 CD34+ cells were plated with 0.1 µM ALRN-6924 or vehicle, and colonies were counted at day 7. *p* values were obtained by t-test; ***, $p < 0.001$; ns, non significant.

(K) *In vivo* treatment of FA-AML1 cells xenografted in NOG-EXL mice. Human FA-AML1 cells were IV-injected 24 hours after receiving 1,25 Gy total body irradiation; after 20 days, mice were randomly assigned to two experimental groups treated intravenously with either 10 mg/kg ALRN-6924 or vehicle 3 times per week for 5 weeks. The percentages of human $CD45^+$ cells in total BM before, and after 2 and 5 weeks of treatment, and in the spleen at sacrifice after 5 weeks of treatment are shown in the left and right graphs, respectively. Each dot is the percentage in a mouse (N=6 and 7 mice in the vehicle and in the ALRN-6924 groups, respectively). *p* values were obtained by the Mann-Whitney test; **, $p < 0.01$; ns, non significant.
See also **Figure S1**.

Figure 6. Canonical bone marrow progression in FA includes a pre-leukemic, 1q+/*MDM4* step of clonal hematopoiesis.

(A) Cumulative incidence in the cohort of 335 FA patients of BM clonal evolution (37% by the age of 40 years) and main recurrent oncogenic lesions (1q+ being the most frequent; 17.6% by the age of 40 years); HSCT and deaths were considered as competitive risks for each event.

(B) Individual longitudinal histories in FA patients with 1q+ clonal evolution. Timeline is shown as a horizontal line (one per patient) from birth to last follow up. Colored boxes underneath show the BM hematologic status according to the revised WHO 2016 classification of myeloid neoplasms. BMF, Bone marrow failure; MDS-MLD, MDS multi-lineage dysplasia (but without excess of blast cells); MDS-EB, MDS with excess of blast cells; AML, acute myeloid leukemia. The main oncogenic lesions are indicated. (C) Bradley-Terry model ranking of the temporal order of the main

oncogenic lesions with respect to blastic progression in the BM (over 5% blast cells). See the Methods section for details on the Bradley-Terry model.

(D) Expression changes in p53 target genes according to the stage of BM progression, normalized on non-FA healthy cells values. From left to right: healthy (non-FA) values, non-clonal FA without overt cytopenia, non-clonal FA at the BMF stage, clonal without blast cells, and clonal with >5% blast cells (MDS-EB/leukemic stage). Healthy and non-clonal stage groups are identical in the left and right graphs. *TP53* target genes for this figure were retrieved from the NEW_FISHER_MEDIUM_SCORE_UP gene set from the census by Fisher[56]. *P* values were obtained by t-test; ***, $p < 0.005$ (α risk with Bonferroni correction).

(E) Expression analysis using RT-qPCR of a set of six main p53 gene targets (*CDKN1A/p21, BAX, GADD45A, PPM1D, SESN2,* and *MAPK14/p38*) assayed in paired BM samples from the same patient, before and after 1q+ (N=5 FA patients). Left panel, data are shown patient-by-patient; right panel, data are shown gene-by-gene with comparison to 5 healthy, non-FA BM samples as controls. Y axis, relative gene expression, normalized on expression of the housekeeping *GAPDH* gene according to the formula: gene level = $2^{[GAPDH\ Ct\ -\ gene\ Ct]}$; expression ranges are shown by vertical bars.

The median gene expression of the 6 grouped target genes was significantly different between the healthy controls and FA before 1q+, and between paired FA before and after 1q+ ($P < 0.005$ by t-test, each).

(F) A model for the canonical, step-wise progression in BM of FA patients that includes the main recurrent somatic chromosomal or molecular events, including 1q+ at the clonal hematopoiesis stage.

See also **Figures S1, S7** and **S8**.

Figure 7. BM clonal evolution and transformation is linear rather than branched in FA.

Clonal architecture was analyzed using combining karyotype, FISH, aCGH and NGS on longitudinal samples. Longitudinal data according to age and Fishplots from four representative FA patients are shown.

STAR*METHODS

RESOURCE AVAILABILITY

Lead contact

Further information and requests for resources and reagents should be directed to and will be fulfilled by the lead contact, Jean Soulier (jean.soulier@aphp.fr).

Materials availability

All unique reagents generated in this study are available from the Lead Contact with a completed Materials Transfer Agreement.

Data and code availability

- This paper analyzes existing, publicly available data. These accession numbers for the datasets are listed in the key resources table. De-identified patient functional genomics data have been deposited at ArrayExpress repository (EMBL-EBI), and accession numbers are listed in the key resources table. They are available upon request if access is granted. To request access, contact DRIVE University Paris-Cité (direction.drive@u-paris.fr).
- All original code has been deposited at GitHub and is publicly available as of the date of publication. DOIs are listed in the key resources table.
- Any additional information required to reanalyze the data reported in this paper is available from the Lead Contact upon request.

EXPERIMENTAL MODEL AND SUBJECT DETAILS

Animal experiments

All mice were housed and handled in the pathogen-free animal facility *Département d'Expérimentation Animale* in accordance with the guidelines of the Animal Care and Use Committee (IRSL, Saint-Louis Hospital, University Paris-Cité). Authorizations for animal experimentation was obtained with the No. 2014-IUH013 and APAFIS#19958-2019032615074625v2, in accordance with French laws.

***Fancg*$^{-/-}$ mice** were a kind gift of F. Arwert[57]. Mice were back-crossed on C57Bl6 background (n > 10 time).

Transgenic mice for the *Mdm4* gene locus *(Mdm4*^{Tg}*)*. To generate the B6J.B6N-Tg(RPL23-203E15).A mouse, thereafter referred *Mdm4*^{Tg}, the 190,044 bp Mouse BAC RPL23-203E15 (ordered at Life technologies SAS), that includes the complete *Mdm4* (also known as *Mdmx*) gene along with 22.006 Kb 5' and 128.726 Kb 3' flanking regions, was micro-injected in the C57BL/6N background. Mice were genotyped using the Phire PCR Kit (Thermo Scientific) and primers pairs ATTTAGGTGACACTATAG (forward) and GGTGGGTGCTAGGTAGGAGA (reverse), and TTGTGGTTTCCCAGTCCCAG (forward) and TAATACGACTCACTATAGGG (reverse). Stable integration of the *Mdm4* BAC was visualized in the *Mdm4*^{Tg} line after several generations crossed with the C57BL/6J using aCGH (Agilent, SurePrint G3 Mouse Genome CGH Microarray 1M). *Mdm4* gene overexpression was checked in mouse tissues by specific RT-qPCR using the CAAGCCCTCTCTATGACATGC and ATCCTGTGCGAGAGCGAGA primers and immunoblotting.

***Fancg*$^{-/-}$*Mdm4*^{Tg} mice** were obtained by crossing *Fancg*$^{-/-}$ and *Mdm4*^{Tg} mice.

Immunodeficient humanized NOG-EXL mice (NOG mice expressing human GM-CSF and IL-3 cytokines, purchased from Taconic Biosciences A/S) were used for xenograft experiments.

Patient cohort

Patients with a suspected or known diagnosis of FA were referred to the laboratory of the French Bone Marrow Failure Center Laboratory at Saint-Louis Hospital, Paris, France. All patients seen between February 2002 and September 2020 with a definitive FA diagnosis (performed using clinical and biological criteria including hypersensitivity to interstrand crosslinker agents in blood cells or skin fibroblasts[66], were included in the present study. Biallelic germline *FANC* mutations or deletions were identified in all the 302 analyzed FA patients (from the 335 FA patient's cohort) using fibroblast DNA prepared after FA diagnosis. The patient database was approved by the French National Data Protection Agency (CNIL, No. 1609899).

Informed consent and authorization for research and cryopreservation were given by the patients or their relatives, in accordance with the Declaration of Helsinki and French law, and IRB approval from the INSERM was given under the number 12-078 to the overall research project.

Patient primary materials

FA patient samples were obtained and cryopreserved with informed content from skin biopsy, blood and bone marrow aspirate at FA diagnosis evaluation. Primary fibroblast cells were grown from skin biopsy in order to get reference non-hematopoietic cells, considered as germline, as previously described[67,68]. Iterative blood and BM samples were subsequently collected and cryopreserved during FA clinical follow up. Thirty-two patients with clonal evolution were previously studied using aCGH and Sanger sequencing of 10 myeloid neoplasm genes[14].

Samples from healthy subjects were obtained with informed consent as controls for genomic analyses and for functional experiments, with informed consent, from the Hematology Laboratory and Biotherapy department of Saint-Louis Hospital, Paris, respectively.

Cell lines

FA-AML1, an AML cell lines derived from a FA-D1/BRCA2 patient that bears a 1q duplication, was kindly obtained from Stefan Meyer (University of Manchester, UK)[58]. The 1q+ and identity of the cell line was confirmed in our laboratory by array-CGH (not shown). FA-AML1 cells were grown in RPMI 1640 medium (Gibco) supplemented with 2mM l-glutamine (Gibco), 1% penicillin/streptomycin (Gibco), 10ng/mL recombinant interleukin-3 (Miltenyi), 1% 5637 cell line supernatant and 20% heat-inactivated fetal calf serum (FCS) (Gibco) in a humidified 5% CO_2 incubator at 37 °C.

The non-FA, *TP53*-mutated, K562 AML cell line was a kind gift of Alexandre Puissant (INSERM, Paris) after identity verification by short tandem repeat loci profiling. K562 was used as negative control cell line for MDM4 inhibitor experiments in standard culture conditions.

All cell lines were tested monthly negative for Mycoplasma using MycoAlert PLUS Mycoplasma Detection Kit (#LT07–705, Lonza) or MycoStrip Mycoplasma Detection Kit (Invivogen, rep-mys-50).

METHOD DETAILS

Patient hematologic features and staging

Bone marrow failure (BMF) was defined when patients presented at least one cytopenia (neutrophil count < 1 G/L, platelet count < 100 G/L and/or Hemoglobin (Hb) concentration < 2 SD below mean, adjusted for age) of central origin confirmed by bone marrow aspiration and/or biopsy. Bone marrow morphological exam was performed at each available timepoint according to the 2016 revision of the World Health Organization (WHO) classification of MDS and AML criteria[69], considering however moderate dyserythropoiesis as a classic sign of FA, but not as a criterion for MDS[66,70]. According to the 2016 revision of the WHO classification, the blast cell % threshold in the BM was > 5% and > 20% for MDS-EB and AML diagnosis, respectively. Results of blood tests and marrow examination were centrally reviewed, and the referring cytologists or pathologists were contacted where necessary; a centralized reviewing of the slide was performed for the 62 patients considered as clonal by at least one expert pathologist from the Aplasia and MDS Saint-Louis and Robert Debré hospitals reference center, Paris.

Array-CGH and single nucleotide polymorphism (SNP)-arrays karyotyping

A high-density copy number analysis of the BM genomic DNA was performed using 180K, 400K or 1M Agilent arrays, Genome-Wide Human SNP Array 6.0 (Affymetrix), and/or GeneChip Mapping 500K Assay (Affymetrix), following the manufacturer recommendations. The final retained copy number lesions were validated by visual analysis by at least two separate expert investigators, considering the size and log2 ratio of the abnormalities with respect to the individual background noise of each array at each particular chromosomal location.

Targeted gene sequencing.

A shared panel of 48 target genes of myeloid malignancy (custom Saint-Louis Hospital MDS/AML panel) was examined for mutations using capture and next-

generation sequencing (see gene list in **Figure 2D**; SureSelect, Agilent; and Illumina). Sequencing data were analyzed for variant calling, using an in-house pipeline as previously described[71], through which high-probability pathogenic mutations were retained by eliminating sequencing/mapping errors and known/possible SNPs based on the available databases and frequencies of variant reads. A VAF threshold of 2% was considered.

Whole-exome sequencing (WES). Whole exome libraries from 13 paired tumoral and fibroblast cell DNAs (total 26 samples) were prepared using SureSelect XT Target Enrichment (Agilent). Sequencing was performed on NextSeq500 systems (Illumina). Data analysis for somatic mutations and CNAs detection was performed using the common Saint-Louis hospital/IRSL pipelines (details available upon request). All detected mutations were also found by panel resequencing except rare mutations that were found at low VAF (2-3%) by panel but undetected by WES due to difference in sequencing depth (mean 913X and 70X in panel sequencing and WES, respectively, limit of detection by WES 5-10% VAF).

The Beat-AML cohort[16] was used as WES AML control and downloaded from the National Cancer Institute (NCI) Genomic Data Commons (GDC) facility, dbGaP Study accession phs001657; we selected 27 paired tumoral and germline cases (total 54 samples) based on age to match the FA clonal cases and processed them using the same WES analysis pipeline.

Whole-genome sequencing (WGS)

DNA of 16 paired AML and fibroblast cell DNAs (total, 32 samples) from FA patients (grouped into 11 *FA core* and 5 *BRCA2*) were prepared using NEBNext Ultra II DNA Library Prep Kit and sequenced on PE 150 pb run on the Illumina NovaSeq600. Thirty AML and non-tumoral pairs (60 samples) of BAM files from the pediatric

TARGET AML cohort, specifically the Illumina-processed WGS files (i.e. the 30 TARGET-21 discovery cases), were obtained as non-FA controls from the NCI GDC portal database (dbGaP Study accession phs000218)[17].

Variant Calling. Sequence reads were mapped to the Human genome build hg38 using the Burrows-Wheeler Aligner (BWA). All BAM alignment files were preprocessed with the Galaxy tool artbio_bam_cleaning (v1.6+galaxy1) to remove low quality alignments and PCR duplicates as well as to left align indels in repeat sequences and recompute MD and NM tags accordingly.

Somatic single nucleotide variations (SNV) and small indels (up to 60 nt) were detected from non-tumoral/tumoral pairs of BWA BAM alignments using the Galaxy tool wrapper varscan_somatic 2.4.3.6 and varscan 2.4.3. Variants called by varscan were further filtered for quality ("PASS" tag) and somatic status (SS tag to 2).

Large somatic deletions, duplications and translocations were detected using the Galaxy tool wrapper lumpy_smoove (v0.2.5+galaxy5) built from the smoove script (https://github.com/brentp/smoove). Smoove makes use of the lumpy algorithm[60] for variant detection and of SVtyper[61] for genotyping. We excluded the potentially misassembled genomic regions listed in the files exclude.cnvnator_100bp.GRCh38.20170403.bed (for FA-core and BRCA2 datasets), and ceph18.b37.lumpy.exclude.2014-01-15.bed (for TARGET datasets) available at https://github.com/hall-lab/speedseq/annotations. Structural variants detected by lumpy_smoove were filtered for Quality > 175 to remove outliers and we selected somatic variants on the basis of their genotype transitions 0/0 in fibroblasts to 0/1 or 1/1 in tumor samples.

Copy Number Alterations were analyzed using the saasCNV R package in the RStudio environment. In brief, both read depth obtained from BAM alignments and

the allelic intensity ratio of variant to reference alleles (B-Allele Frequencies) obtained from the VCF varscan outputs were used with a joint segmentation approach to identify, in normal-tumor pairs, the boundaries of genomic segments with copy number alterations. Adjacent segments were merged when their copy numbers did not significantly differ (X^2-test). Gain and loss status were assigned when the copy number was respectively greater and lower than the baseline, and copy neutral loss of heterozygosity (LOH) was assigned when the copy number was unchanged from the baseline while the allelic imbalance was showing the loss of an allele. Genomic boundaries of the copy number alterations were further curated manually to refine their location and discard low change alterations.

Analysis of somatic mutation sizes. Somatic variants were counted for different size ranges. Lumpy_smoove VCF outputs were used to count [1Kb - 1Mb[variants, respectively. Variants detected in a common set of regions involved in large CNAs > 1Mb were excluded from the overall analysis to avoid comparison bias. Distributions of mutation size were visualized using RStudio (R version 3.6.1) and ggplot2 (3.3.2). To assess the differences between variant size distributions in FA-Core, BRCA2 and TARGET (non-FA) groups, statistical tests were performed using the t-test from stat_compare_means function of the R package ggpubr (0.4.0).

Tumor mutational burdens (TMBs) were computed as described with minor modifications[72]. Thus, the numbers of single nucleotide variations and small indels per megabases of exonic sequences were computed from the VCF files generated by varscan after excluding known germline alterations in the build 153 of dbSNP as well as somatic variants associated with a p-value > 0.05 in Fisher's exact test (SPV tag in the varscan VCF files).

Cosmic mutational signatures (v3.2 - March 2021) were generated from the varscan VCF files and visualized using the R package MutationalPatterns wrapped in the Galaxy tool mutational_patterns (v2.0.0+galaxy13.1). As the TARGET-21 BAM alignments were obtained with the human reference genome hg19, coordinates in the corresponding VCF files were converted to the hg38 reference using the Galaxy tool crossmap_vcf (v0.3.7+galaxy1) and the CrossMap software before analysis of their mutational signatures. This allowed proper comparison with mutational signatures in the *FA core* and *BRCA2* datasets. Unrooted clustering of mutational signatures was performed with the Galaxy wrapper high_dim_heatmap (v1.1.0) using the functions hclust and heatmap.2 of the gplots R package, the Euclidean distance method and the Average clustering method.

To confirm the relevance of the identified signatures, *de novo* mutational signatures were extracted using the function extract_signatures of MutationalPatterns on a mutation matrix including the BRCA2, FA core and TARGET case datasets, after determining the optimal factorization rank to 3 with the NMF (Nonnegative Matrix Factorization) R package. The number of runs for fitting the best signatures was set to 60. The efficacy of the *de novo* signatures in reconstructing the mutational patterns in datasets was estimated using the cosine similarity of original *versus* reconstructed datasets. Each *de novo* signature was renamed according to the name of the COSMIC v3.2 signature with the best cosine similarity, SBS1-like, SBS3-like and SBS5-like having a cosine similarity of 0.83, 0.91 and 0.77 with their COSMIC counterparts, respectively.

Scripts for variant analysis, copy number alterations, tumor burden, cosmic mutational signatures on WGS data are available in https://github.com/ARTbio/tools-artbio/tree/master/scripts.

HRDetect signatures were computed using the HRDetect-pipeline[73] available at https://github.com/eyzhao/hrdetect-pipeline. We first processed the TARGET-21 dataset using the Galaxy workflow prepare_for_hg19-HRDetect.ga. Briefly, 4 types of files were generated. The somatic short indels (somatic_indels.vcf) and the somatic single nucleotide variations (somatic_snvs.vcf) were obtained from the somatic_varscan vcf files previously generated. The large structural variants (somatic_sv.tsv) were obtained from the lumpy_smoove vcf files previously generated using the Galaxy tool "Convert lumpy-smoove vcf to tabular hrdetect" (Galaxy Version 1). Finally, the CNAs and LOH (segments.tsv) were compiled from the raw somatic-varscan vcf files using the Galaxy tool "Infer CNVs from SNVs" (Galaxy Version 0.7.0). To process the sequence datasets, we used the Galaxy workflow Galaxy-Workflow-Prepare_hg38_for_hg19-HRDetect.ga which generated the 4 types of files (somatic_indels.vcf, somatic_snvs.vcf, somatic_sv.tsv and segments.tsv) in the same way, except that coordinates of these variations were cross-mapped from hg38 to hg19 references. Files were then loaded into a local implementation of the hrdetect-pipeline (https://github.com/ARTbio/hrdetect-pipeline) and processed as recommended. Outputs were plotted using ggplot2; **, $p \leq 0.01$; ****, $p \leq 0.0001$, by t-test.

Translocation breakpoint junction sequencing

Ten FA AML were specifically analyzed using WGS to characterize the translocation breakpoint junctions (**Table S3**). Sequence reads were mapped to the human genome hg19/GRCh37 (repeat unmasked) using BWA Fast and accurate short read alignment with Burrows–Wheeler transform (v0.7.4). Duplicates reads were removed using the function MarkDuplicates from Picard tools (v1.94) and a filtering for uniquely mapped reads was performed. Structural variants breakpoints were

identified using SVDetect (v0.8b)[62], Socrates[64], Delly (v0.6.7)[63] and Meerkat (v0.185)[27] tools, and the translocations breakpoints were analyzed in combination with the BM karyotype and aCGH information. Socrates and Meerkat were used to predict nucleotide micro-homologies and untemplated sequences at breakpoints. PCR and Sanger sequencing was performed to confirm the junctions using primer pairs designed using the flanking sequences of the overlapping runs. CNAs were detected with the Control-FREEC algorithm (v6.3) using the hg19 GC content to normalise tumor read coverage[65].

FISH probes. The chromosome 1q centromeric (CENP-A) and 1q12 pericentromeric, (RP11-32326G211) probes were obtained from Abbott (www.molecular.abbott) and Life technologies (www.thermofisher.com), respectively.

RNA-seq study, transcriptome and gene fusion analysis

RNAs were extracted from frozen pellets obtained after sorting the CD14+ blood cells of 56 FA patients (70 samples, including longitudinal samples in 12 patients) and 9 healthy controls (**Table S8**). We used blood CD14+ cells, i.e. the monocytic fraction, to overcome the heterogeneity in the FA bone marrow related to dyserythropoiesis, hypoplasia or blast cells, as well as the relative lack of CD34+ cells that characterizes the BMF stage in FA[10]. Importantly, we found that blood CD14+ cells harbored the same chromosomal abnormalities as the BM cells, showing that they readily represent the clonal hematopoietic population (**Figure S5B**). Samples at the various stages of hematopoietic FA evolution, i.e. non-clonal FA without overt cytopenia, non-clonal FA with overt bone marrow failure, clonal FA with BM blasts < 5%, clonal FA with BM blasts ≥ 5%, and healthy non-FA controls were used (**Tables S3** and **S8**). This approach enabled us to robustly compare gene expression in consistent cells at various stages of the disease.

Libraries for RNA-seq were prepared using the Clontech®Smarter Stranded RNA Seq. Ribo-Zero Gold and PE sequencing was performed using HiSeq4000 (Illumina). A subset of 500,000 reads from each FASTQ file was aligned to the reference human genome hg19/GRCh37, with TopHat2 to determine insert sizes (www.broadinstitute.github.io/picard/). Read mapping to multiple locations were removed. HTSeq[74] was used to obtain the number of reads associated with each gene in the Gencode database (restricted to protein-coding genes, antisense and lincRNAs). The Bioconductor DESeq2 package was used to import raw HTSeq counts for each sample into R statistical software and extract the count matrix. After normalizing for library size, the count matrix was normalized by the coding length of genes to compute FPKM scores (number of fragments per kilobase of exon model and millions of mapped reads). Final scores were obtained by Log2(x+1) transformation and quantile normalization.

Gene set enrichment analyses (GSEA) was performed for the MSigDBhallmarks gene sets and custom gene sets (described in the Figure legend), using the Broad Institute software application (software.broadinstitute.org/gsea/download.jsp). The NEW_FISHER_MEDIUM_SCORE_UP gene set list was retrieved from the census by Fisher[56].

Gene fusions were detected using FusionCatcher (www.github.com/ndaniel/fusioncatcher).

Individual gene expression in a number of p53 gene targets were assayed using RT-qPCR. Primers were *CDKN1A/p21*, AGTCAGTTCCTTGTGGAGCC and GCATGGGTTCTGACGGACAT; *SESN2* ATATCCACTGCGTCTTTGGCA and GGTCTTCTCTGGGTAGCAGG; *PPM1D*, TCAATGTGCCAGGACCAAGA and GCCCAATGCTCGATTCACAAG; *BAX*, CAAGACCAGGGTGGTTGG and

CACTCCCGCCACAAAGAT; *P38MAPK*/*MAPK14,* TCTCATTAACAGGATGCCAAGC and ACAAGCATCTTCTCCAGCAAGT; *GADD45A*, GCTCTTGGAGACCGACGC and CGACTTTCCCGGCAAAAACAAA.

Colony-Forming Unit Granulocytes/Macrophage (CFU-GM) assays

CFU-GM assays were performed in patient or murine cells as we previously described with minor modifications[10]. Cells were plated and cultured in MethoCult medium (Stem Cell Technologies) and colonies were counted using standard criteria on the day indicated in the legend. Cells for **Figure 4E** and **4F** were lentivirally transduced using lentiviral particles produced as described below and as shown in the figure (see legend).

Plasmid and lentiviral gene transfer for gene expression modulation

The human *MDM4* and the murine *Mdm4 (*also known as *Mdmx)* cDNAs, a kind gift from R. Fahraeus[59], were subcloned in the pTRIP-EF1α-GFP vector and transduced using lentivirus. We previously described the Hu ShRNA anti-*TP53* and Mu ShRNA anti-*Tp53*[10]. Murine anti-Fancd2 and control shRNAs were purchased from TransOmic Technologies (references TLMSU1400, Fancd2 pZIP hEF1α turboRFP, and TLM SU4430, ultra mir shRNA NTp ZIP hEF1α ZsGreen Puro, respectively). Human anti-*MDM4* and controls shRNAs were purchased from TransOmic Technologies (references TLHSU1418, ultra mir shRNA MDM4-56 or -59 pZIP hEF1α ZsGreen Puro, and TLM SU4430, ultra mir shRNA NT pZIP hEF1α ZsGreen Puro, respectively).

Lentiviral particles were produced with jetPRIME reagents (Polyplus transfection) by co-transfection of viral production plasmids in T150 cm^2 tissue culture flasks containing $2x10^6$ HEK-293T cells by flask, according to the manufacturer's protocol.

Viral supernatants were filtered through a 0.45um HV Durapore membrane (Merck Millipore) and concentrated by ultra-centrifugation at 24,000 rpm for two hours at 4°C, and stored at -80°C.

Primary patient or murine cells were transduced overnight for 16 hours with the lentiviral supernatants including controls. Efficient gene overexpression or silencing was checked using specific immunoblot using antibodies against murine Mdm4 (Abcam Antibody), human HDMX/MDM4 (A300-287A, Bethyl Laboratories), murine Fancd2 (R&D Systems), a polyclonal Ab to human and murine FANCD2 (kind gift from KJ Patel), human p53 (D0-1, Santa Cruz), murine p53 (Calbiochem, clone PAb240), and antibodies against Actin (Santa Cruz), Vinculin (Abcam) or GAPDH (Sigma) as loading controls; in addition, expression of murine *Mdm4* and *Fancd2* was tested by RT-qPCR using primers TCTGGGAGAAGCCACGTAGA and CCTCAATGTCCAGCTCTCGG (*Mdm4*), and CAAGCCCTCTCTATGACATGC and ATCCTGTGCGAGAGCGAGA (*Fancd2*). Polyclonal antibodies against human phospho-p53 (S15 P-p53) and monoclonal antibodies against human p21 were used (Cell Signaling Technology, #9284 and #2947, respectively).

FA-AML1 cells were transduced overnight for 16 hours with the lentiviral supernatants anti-MDM4 and controls produced as described below, then washed and cultivated for 48h. Immunoblotting were assayed on ZsGreen-sorted cells.

Competitive graft of *Mdm4^{Tg}* or WT cells after lentiviral knockdown of *Fancd2* (FA-like cells). BM cells were harvested from eight- to twelve-week-old wild-type Ly5.1 (CD45.1) and *Mdm4^{Tg}* (CD45.2) C57BL/6 mice. Lin- progenitor cells were prepared using Mouse Lineage Cell Depletion Kit (Miltenyi Biotech) and were transduced overnight for 16 hours with shRNA Fancd2-RFP or NT-ZsGreen lentivector (see Plasmid and lentiviral gene transfer section above) at a MOI

(multiplicity of infection) of 50-200 IU/cell. $4x10^5$ of these cells were IV-injected with various ratios of *Mdm4*^{Tg} and WT cells into the tail vein of lethally irradiated (9 Gy) C57BL6/J female mice (n=5 mice in experiment shown Figures 4H and S6E; n= 6 mice in experiment shown Figure S6F,G). Cells were stained with APC anti-mouse CD45.2 (Clone A20), BV510 anti-mouse CD45.1 (Clone104) antibodies, all from BD Biosciences. Flow cytometry analysis were performed on a FACS Aria III cell sorter (Beckton Dickinson) and a Fortessa Analyzer (Beckton Dickinson).

Chronic stress-induced bone marrow failure in genetically modified mice. Mice from the 4 genotypes, aged 8-12 weeks, were intraperitoneally injected with 5mg/kg of Poly(I:C) HMW (Invivogen), twice a week for 8 cycles of injections (4 weeks of injection –8 injections–, followed by 4 weeks of recovery)[13]. Blood counts in all mice were analyzed every 4 weeks using the automated analyzer (MS9-5, Melet Schloesing Laboratories).

In vitro drug testing

For viability and cell cycle analysis, FA-AML1 and K562 cells were incubated in triplicate with the MDM4 inhibitors SJ-172550 (purchased from Sigma-Aldrich) or ALRN-6924 (provided to P.F. and J.S. from Aileron Therapeutics, Cambridge, MA, USA)[32], at IC-50 (50µM and 1.8µM, respectively, as defined by MTT assay in liquid culture, data not shown) and DMSO for 24, 48 and 72 hours in a humidified 5% CO_2 incubator at 37°C. Survival, apoptosis and cell cycle were analyzed on ZsGreen-gated cells using Annexin V-FITC kit. Briefly, cells were washed, incubated with Annexin V-FITC antibody (Miltenyi Biotec) for 20 minutes, washed twice, incubated with Propidium Iodide and analyzed using FACSCanto (BD Biosciences) and Flowjo 10.1 (TreeStar). Cell cycle was monitored using APC BrdU Flow kit (BD Pharmigen). Briefly, cells were incubated for with 1mM BrdU for two hours at 37 °C. Cells were

then fixed, permeabilized and incubated with 300µg/ml DNase for one hour at 37 °C. Cells were incubated with BrdU-APC antibody for 20 min, Vybrant violet (Invitrogen) for 30 min at 37°C and analyzed using FACSCanto (BD Biosciences) and Flowjo 10.1 (TreeStar).

Methylcellulose replating assays in FA-AML1 cell line was performed using ClonaCell-TCS Medium (StemCell). FA-AML1 cells were seeded at 200 cells by well in 24 wells plate in triplicate, with SJ-172550 or ALRN-6924 MDM4 inhibitors at 0.1µM, 0.01µM, 0.001µM or DMSO in a humidified 5% CO_2 incubator at 37°C. After 10 days, the number of colonies was scored, and cells were harvested and replated in fresh ClonaCell-TCS medium in the same conditions as before for 10 days, until exhaustion of colonies.

Human primary 1q+ or non-1q AML cells from FA patients were tested upon ALRN-6924 exposure for CFU assay. 10^4 CD34+ BM cells were plated (N=7 each) upon 0.1 µM ALRN-6924 or vehicle, and colonies were counted at day 7 using standard criteria.

Xenograft treatment experiments. Human 1q+ FA-AML1 cells were xenografted in NOG-EXL mice. 10^6 FA-AML1 cells were IV-injected in N=13 female, 8 week-old NOG-EXL mice 24 hours after 1,25 Gy total body irradiation; after 20 days, mice were randomly assigned to two experimental groups treated intravenously with either 10 mg/kg ALRN-6924 or vehicle PBS 3 times per week for 5 weeks (N=6 and 7 mice, respectively). The percentages of human CD45+ cells in total BM before, and after 2 and 5 weeks of treatment, and in the spleen at sacrifice after 5 weeks of treatment were analysed.

QUANTIFICATION AND STATISTICAL ANALYSIS

Clinical analyses and statistics

All statistical analyses were performed using the R software (version 4.1.1) (www.R-project.org/). All included patients with a FA diagnosis were analyzed.

All tests were two-sided and p values below 0.05 defined statistical significance. Summary statistics, namely median with interquartile range (IQR), or percentages, were computed according to the type of variable.

Overall survival was computed using the Kaplan-Meier method. Cumulative incidence of each event (namely, blastic or clonal progression) was estimated in a competing risks framework to handle deaths prior to those events of interest. Survival probabilities were computed whether or not the patients underwent HSCT. All time-to-failure data were expressed on the age scale. Comparison of survival curves according to clonal progression used the Simon and Makuch method to handle the time to occurrence of the clonal event[75]; test comparison uses the Mantel-Byar test for comparison of survival data with the time dependent covariate, that is, the clonal evolution that occurs at different age.

More statisticall details of the cohort analysis including numbers of patients exposed to the tisk (No at risk) and confidence range can be found in the legend of Figure 1.

The relative timing of the main oncogenic lesions in the entire FA cohort was analyzed in **Figure 6C** using the global Bradley and Terry model[76]. The global Bradley and Terry model is a probability model that can predict the outcome of a paired comparison (i and j); it was first proposed in 1952 to describe the probability that one treatment is preferred to another. The pairwise comparison ‘i>j’ can be read as ‘i is preferred to j’, ‘i beats j’ or ‘i ranks higher than j’, depending on the application.

We applied the model to the age of occurrence of the main oncogenic lesions with respect to BM blastic progression, providing a ranking of those events.

General statistical information

Statistical analyses were performed with GraphPad Prism (GraphPad Software). Data are expressed as average +/- standard deviation (SD). Unless otherwise noted, a paired nonparametric test was used to assess significance. Details on type of tests uses were specified in the legend of each figure. Asterisks denote p-values as follows: $*$ $p < 0.05$; $**$ $p < 0.01$; $***$ $p < 0.001$. Each N represents alternatively a patient's sample or a biological replicate as detailed in the legend of each figure.

REFERENCES

1. Ceccaldi, R., Sarangi, P., and D'Andrea, A.D. (2016). The Fanconi anaemia pathway: new players and new functions. Nat. Rev. Mol. Cell Biol. *17*, 337–349. 10.1038/nrm.2016.48.

2. Shimamura, A., and Alter, B.P. (2010). Pathophysiology and management of inherited bone marrow failure syndromes. Blood Rev. *24*, 101–122. 10.1016/j.blre.2010.03.002.

3. Peffault de Latour, R., Porcher, R., Dalle, J.-H., Aljurf, M., Korthof, E.T., Svahn, J., Willemze, R., Barrenetxea, C., Mialou, V., Soulier, J., et al. (2013). Allogeneic hematopoietic stem cell transplantation in Fanconi anemia: the European Group for Blood and Marrow Transplantation experience. Blood *122*, 4279–4286. 10.1182/blood-2013-01-479733.

4. Butturini, A., Gale, R.P., Verlander, P.C., Adler-Brecher, B., Gillio, A.P., and Auerbach, A.D. (1994). Hematologic abnormalities in Fanconi anemia: an International Fanconi Anemia Registry study. Blood *84*, 1650–1655.

5. Kutler, D.I., Singh, B., Satagopan, J., Batish, S.D., Berwick, M., Giampietro, P.F., Hanenberg, H., and Auerbach, A.D. (2003). A 20-year perspective on the International Fanconi Anemia Registry (IFAR). Blood *101*, 1249–1256. 10.1182/blood-2002-07-2170.

6. Rosenberg, P.S., Socié, G., Alter, B.P., and Gluckman, E. (2005). Risk of head and neck squamous cell cancer and death in patients with Fanconi anemia who did and did not receive transplants. Blood *105*, 67–73. 10.1182/blood-2004-04-1652.

7. Wagner, J.E., Tolar, J., Levran, O., Scholl, T., Deffenbaugh, A., Satagopan, J., Ben-Porat, L., Mah, K., Batish, S.D., Kutler, D.I., et al. (2004). Germline mutations in BRCA2: shared genetic susceptibility to breast cancer, early onset leukemia, and Fanconi anemia. Blood *103*, 3226–3229. 10.1182/blood-2003-09-3138.

8. Mitchell, R., Wagner, J.E., Hirsch, B., DeFor, T.E., Zierhut, H., and MacMillan, M.L. (2014). Haematopoietic cell transplantation for acute leukaemia and advanced myelodysplastic syndrome in Fanconi anaemia. Br. J. Haematol. *164*, 384–395. 10.1111/bjh.12634.

9. Peffault de Latour, R., and Soulier, J. (2016). How I treat MDS and AML in Fanconi anemia. Blood *127*, 2971–2979. 10.1182/blood-2016-01-583625.

10. Ceccaldi, R., Parmar, K., Mouly, E., Delord, M., Kim, J.M., Regairaz, M., Pla, M., Vasquez, N., Zhang, Q.-S., Pondarre, C., et al. (2012). Bone marrow failure in Fanconi anemia is triggered by an exacerbated p53/p21 DNA damage response that

impairs hematopoietic stem and progenitor cells. Cell Stem Cell *11*, 36–49. 10.1016/j.stem.2012.05.013.

11. Garaycoechea, J.I., Crossan, G.P., Langevin, F., Mulderrig, L., Louzada, S., Yang, F., Guilbaud, G., Park, N., Roerink, S., Nik-Zainal, S., et al. (2018). Alcohol and endogenous aldehydes damage chromosomes and mutate stem cells. Nature *553*, 171–177. 10.1038/nature25154.

12. Rodríguez, A., Zhang, K., Färkkilä, A., Filiatrault, J., Yang, C., Velázquez, M., Furutani, E., Goldman, D.C., García de Teresa, B., Garza-Mayén, G., et al. (2020). MYC Promotes Bone Marrow Stem Cell Dysfunction in Fanconi Anemia. Cell Stem Cell, 33–47. 10.1016/j.stem.2020.09.004.

13. Walter, D., Lier, A., Geiselhart, A., Thalheimer, F.B., Huntscha, S., Sobotta, M.C., Moehrle, B., Brocks, D., Bayindir, I., Kaschutnig, P., et al. (2015). Exit from dormancy provokes DNA-damage-induced attrition in haematopoietic stem cells. Nature *520*, 549–552. 10.1038/nature14131.

14. Quentin, S., Cuccuini, W., Ceccaldi, R., Nibourel, O., Pondarre, C., Pagès, M.-P., Vasquez, N., Dubois d'Enghien, C., Larghero, J., Peffault de Latour, R., et al. (2011). Myelodysplasia and leukemia of Fanconi anemia are associated with a specific pattern of genomic abnormalities that includes cryptic RUNX1/AML1 lesions. Blood *117*, e161-170. 10.1182/blood-2010-09-308726.

15. Meyer, S., Bristow, C., Wappett, M., Pepper, S., Whetton, A.D., Hanenberg, H., Neitzel, H., Wlodarski, M.W., Ebell, W., and Tönnies, H. (2011). Fanconi anemia (FA)-associated 3q gains in leukemic transformation consistently target EVI1, but do not affect low TERC expression in FA. Blood *117*, 6047–6050. 10.1182/blood-2011-03-343897.

16. Tyner, J.W., Tognon, C.E., Bottomly, D., Wilmot, B., Kurtz, S.E., Savage, S.L., Long, N., Schultz, A.R., Traer, E., Abel, M., et al. (2018). Functional genomic landscape of acute myeloid leukaemia. Nature *562*, 526–531. 10.1038/s41586-018-0623-z.

17. Bolouri, H., Farrar, J.E., Triche, T., Ries, R.E., Lim, E.L., Alonzo, T.A., Ma, Y., Moore, R., Mungall, A.J., Marra, M.A., et al. (2018). The molecular landscape of pediatric acute myeloid leukemia reveals recurrent structural alterations and age-specific mutational interactions. Nat. Med. *24*, 103–112. 10.1038/nm.4439.

18. Kaneko, H., Misawa, S., Horiike, S., Nakai, H., and Kashima, K. (1995). TP53 mutations emerge at early phase of myelodysplastic syndrome and are associated with complex chromosomal abnormalities. Blood *85*, 2189–2193.

19. Papaemmanuil, E., Gerstung, M., Malcovati, L., Tauro, S., Gundem, G., Van Loo, P., Yoon, C.J., Ellis, P., Wedge, D.C., Pellagatti, A., et al. (2013). Clinical and biological implications of driver mutations in myelodysplastic syndromes. Blood *122*,

3616–3627. 10.1182/blood-2013-08-518886.

20. Rücker, F.G., Schlenk, R.F., Bullinger, L., Kayser, S., Teleanu, V., Kett, H., Habdank, M., Kugler, C.-M., Holzmann, K., Gaidzik, V.I., et al. (2012). TP53 alterations in acute myeloid leukemia with complex karyotype correlate with specific copy number alterations, monosomal karyotype, and dismal outcome. Blood *119*, 2114–2121. 10.1182/blood-2011-08-375758.

21. Li, Y., Roberts, N.D., Wala, J.A., Shapira, O., Schumacher, S.E., Kumar, K., Khurana, E., Waszak, S., Korbel, J.O., Haber, J.E., et al. (2020). Patterns of somatic structural variation in human cancer genomes. Nature *578*, 112–121. 10.1038/s41586-019-1913-9.

22. Alexandrov, L.B., Nik-Zainal, S., Wedge, D.C., Aparicio, S.A.J.R., Behjati, S., Biankin, A.V., Bignell, G.R., Bolli, N., Borg, A., Børresen-Dale, A.-L., et al. (2013). Signatures of mutational processes in human cancer. Nature *500*, 415–421. 10.1038/nature12477.

23. Alexandrov, L.B., Kim, J., Haradhvala, N.J., Huang, M.N., Tian Ng, A.W., Wu, Y., Boot, A., Covington, K.R., Gordenin, D.A., Bergstrom, E.N., et al. (2020). The repertoire of mutational signatures in human cancer. Nature *578*, 94–101. 10.1038/s41586-020-1943-3.

24. Degasperi, A., Amarante, T.D., Czarnecki, J., Shooter, S., Zou, X., Glodzik, D., Morganella, S., Nanda, A.S., Badja, C., Koh, G., et al. (2020). A practical framework and online tool for mutational signature analyses show inter-tissue variation and driver dependencies. Nat. Cancer *1*, 249–263. 10.1038/s43018-020-0027-5.

25. Nik-Zainal, S., Davies, H., Staaf, J., Ramakrishna, M., Glodzik, D., Zou, X., Martincorena, I., Alexandrov, L.B., Martin, S., Wedge, D.C., et al. (2016). Landscape of somatic mutations in 560 breast cancer whole-genome sequences. Nature *534*, 47–54. 10.1038/nature17676.

26. Davies, H., Glodzik, D., Morganella, S., Yates, L.R., Staaf, J., Zou, X., Ramakrishna, M., Martin, S., Boyault, S., Sieuwerts, A.M., et al. (2017). HRDetect is a predictor of BRCA1 and BRCA2 deficiency based on mutational signatures. Nat. Med. *23*, 517–525. 10.1038/nm.4292.

27. Yang, L., Luquette, L.J., Gehlenborg, N., Xi, R., Haseley, P.S., Hsieh, C.-H., Zhang, C., Ren, X., Protopopov, A., Chin, L., et al. (2013). Diverse mechanisms of somatic structural variations in human cancer genomes. Cell *153*, 919–929. 10.1016/j.cell.2013.04.010.

28. Scully, R., Panday, A., Elango, R., and Willis, N.A. (2019). DNA double-strand break repair-pathway choice in somatic mammalian cells. Nat. Rev. Mol. Cell Biol. *20*, 698–714. 10.1038/s41580-019-0152-0.

29. Dutrillaux, B., Couturier, J., Viegas-Péquignot, E., and Schaison, G. (1977). Localization chromatid breaks in Fanconi's anemia, using three consecutive stains. Hum. Genet. *37*, 65–71. 10.1007/BF00293773.

30. Schoder, C., Liehr, T., Velleuer, E., Wilhelm, K., Blaurock, N., Weise, A., and Mrasek, K. (2010). New aspects on chromosomal instability: chromosomal break-points in Fanconi anemia patients co-localize on the molecular level with fragile sites. Int. J. Oncol. *36*, 307–312.

31. Richard, G.-F., Kerrest, A., and Dujon, B. (2008). Comparative genomics and molecular dynamics of DNA repeats in eukaryotes. Microbiol. Mol. Biol. Rev. *72*, 686–727. 10.1128/MMBR.00011-08.

32. Carvajal, L.A., Neriah, D.B., Senecal, A., Benard, L., Thiruthuvanathan, V., Yatsenko, T., Narayanagari, S.-R., Wheat, J.C., Todorova, T.I., Mitchell, K., et al. (2018). Dual inhibition of MDMX and MDM2 as a therapeutic strategy in leukemia. Sci. Transl. Med. *10*, eaao3003. 10.1126/scitranslmed.aao3003.

33. Danovi, D., Meulmeester, E., Pasini, D., Migliorini, D., Capra, M., Frenk, R., de Graaf, P., Francoz, S., Gasparini, P., Gobbi, A., et al. (2004). Amplification of Mdmx (or Mdm4) directly contributes to tumor formation by inhibiting p53 tumor suppressor activity. Mol. Cell. Biol. *24*, 5835–5843. 10.1128/MCB.24.13.5835-5843.2004.

34. Ueda, K., Kumari, R., Schwenger, E., Wheat, J.C., Bohorquez, O., Narayanagari, S.-R., Taylor, S.J., Carvajal, L.A., Pradhan, K., Bartholdy, B., et al. (2021). MDMX acts as a pervasive preleukemic-to-acute myeloid leukemia transition mechanism. Cancer Cell, 529–547. 10.1016/j.ccell.2021.02.006.

35. Wade, M., Li, Y.-C., and Wahl, G.M. (2013). MDM2, MDMX and p53 in oncogenesis and cancer therapy. Nat. Rev. Cancer *13*, 83–96. 10.1038/nrc3430.

36. Köhnke, T., and Majeti, R. (2021). Clonal Hematopoiesis: From Mechanisms to Clinical Intervention. Cancer Discov. *11*, 2987–2997. 10.1158/2159-8290.CD-21-0901.

37. Steensma, D.P., Bejar, R., Jaiswal, S., Lindsley, R.C., Sekeres, M.A., Hasserjian, R.P., and Ebert, B.L. (2015). Clonal hematopoiesis of indeterminate potential and its distinction from myelodysplastic syndromes. Blood *126*, 9–16. 10.1182/blood-2015-03-631747.

38. Warren, J.T., and Link, D.C. (2020). Clonal hematopoiesis and risk for hematologic malignancy. Blood *136*, 1599–1605. 10.1182/blood.2019000991.

39. Laurie, C.C., Laurie, C.A., Rice, K., Doheny, K.F., Zelnick, L.R., McHugh, C.P., Ling, H., Hetrick, K.N., Pugh, E.W., Amos, C., et al. (2012). Detectable clonal mosaicism from birth to old age and its relationship to cancer. Nat. Genet. *44*, 642–650. 10.1038/ng.2271.

40. Jacobs, K.B., Yeager, M., Zhou, W., Wacholder, S., Wang, Z., Rodriguez-Santiago, B., Hutchinson, A., Deng, X., Liu, C., Horner, M.-J., et al. (2012). Detectable clonal mosaicism and its relationship to aging and cancer. Nat. Genet. *44*, 651–658. 10.1038/ng.2270.

41. Dunbar, A.J., Rampal, R.K., and Levine, R. (2020). Leukemia secondary to myeloproliferative neoplasms. Blood *136*, 61–70. 10.1182/blood.2019000943.

42. Kennedy, A.L., Myers, K.C., Bowman, J., Gibson, C.J., Camarda, N.D., Furutani, E., Muscato, G.M., Klein, R.H., Ballotti, K., Liu, S., et al. (2021). Distinct genetic pathways define pre-malignant versus compensatory clonal hematopoiesis in Shwachman-Diamond syndrome. Nat. Commun. *12*, 1334. 10.1038/s41467-021-21588-4.

43. Sarasin, A., Quentin, S., Droin, N., Sahbatou, M., Saada, V., Auger, N., Boursin, Y., Dessen, P., Raimbault, A., Asnafi, V., et al. (2019). Familial predisposition to TP53/complex karyotype MDS and leukemia in DNA repair-deficient xeroderma pigmentosum. Blood *133*, 2718–2724. 10.1182/blood-2019-01-895698.

44. Wong, T.N., Miller, C.A., Jotte, M.R.M., Bagegni, N., Baty, J.D., Schmidt, A.P., Cashen, A.F., Duncavage, E.J., Helton, N.M., Fiala, M., et al. (2018). Cellular stressors contribute to the expansion of hematopoietic clones of varying leukemic potential. Nat. Commun. *9*, 455. 10.1038/s41467-018-02858-0.

45. Menssen, A.J., and Walter, M.J. (2020). Genetics of progression from MDS to secondary leukemia. Blood *136*, 50–60. 10.1182/blood.2019000942.

46. Yurchenko, A.A., Padioleau, I., Matkarimov, B.T., Soulier, J., Sarasin, A., and Nikolaev, S. (2020). XPC deficiency increases risk of hematologic malignancies through mutator phenotype and characteristic mutational signature. Nat. Commun. *11*, 5834. 10.1038/s41467-020-19633-9.

47. Mirchandani, K.D., McCaffrey, R.M., and D'Andrea, A.D. (2008). The Fanconi anemia core complex is required for efficient point mutagenesis and Rev1 foci assembly. DNA Repair *7*, 902–911. 10.1016/j.dnarep.2008.03.001.

48. Papadopoulo, D., Guillouf, C., Mohrenweiser, H., and Moustacchi, E. (1990). Hypomutability in Fanconi anemia cells is associated with increased deletion frequency at the HPRT locus. Proc. Natl. Acad. Sci. U. S. A. *87*, 8383–8387. 10.1073/pnas.87.21.8383.

49. Zou, X., Owusu, M., Harris, R., Jackson, S.P., Loizou, J.I., and Nik-Zainal, S. (2018). Validating the concept of mutational signatures with isogenic cell models. Nat. Commun. *9*, 1744. 10.1038/s41467-018-04052-8.

50. Howlett, N.G., Taniguchi, T., Durkin, S.G., D'Andrea, A.D., and Glover, T.W. (2005). The Fanconi anemia pathway is required for the DNA replication stress

response and for the regulation of common fragile site stability. Hum. Mol. Genet. *14*, 693–701. 10.1093/hmg/ddi065.

51. Madireddy, A., Kosiyatrakul, S.T., Boisvert, R.A., Herrera-Moyano, E., García-Rubio, M.L., Gerhardt, J., Vuono, E.A., Owen, N., Yan, Z., Olson, S., et al. (2016). FANCD2 Facilitates Replication through Common Fragile Sites. Mol. Cell *64*, 388–404. 10.1016/j.molcel.2016.09.017.

52. Soto, M., Raaijmakers, J.A., Bakker, B., Spierings, D.C.J., Lansdorp, P.M., Foijer, F., and Medema, R.H. (2017). p53 Prohibits Propagation of Chromosome Segregation Errors that Produce Structural Aneuploidies. Cell Rep. *19*, 2423–2431. 10.1016/j.celrep.2017.05.055.

53. Lord, C.J., and Ashworth, A. (2016). BRCAness revisited. Nat. Rev. Cancer *16*, 110–120. 10.1038/nrc.2015.21.

54. Río, P., Navarro, S., Wang, W., Sánchez-Domínguez, R., Pujol, R.M., Segovia, J.C., Bogliolo, M., Merino, E., Wu, N., Salgado, R., et al. (2019). Successful engraftment of gene-corrected hematopoietic stem cells in non-conditioned patients with Fanconi anemia. Nat. Med. *25*, 1396–1401. 10.1038/s41591-019-0550-z.

55. Davoli, T., Xu, A.W., Mengwasser, K.E., Sack, L.M., Yoon, J.C., Park, P.J., and Elledge, S.J. (2013). Cumulative haploinsufficiency and triplosensitivity drive aneuploidy patterns and shape the cancer genome. Cell *155*, 948–962. 10.1016/j.cell.2013.10.011.

56. Fischer, M. (2017). Census and evaluation of p53 target genes. Oncogene *36*, 3943–3956. 10.1038/onc.2016.502.

57. Koomen, M., Cheng, N.C., van de Vrugt, H.J., Godthelp, B.C., van der Valk, M.A., Oostra, A.B., Zdzienicka, M.Z., Joenje, H., and Arwert, F. (2002). Reduced fertility and hypersensitivity to mitomycin C characterize Fancg/Xrcc9 null mice. Hum. Mol. Genet. *11*, 273–281. 10.1093/hmg/11.3.273.

58. Meyer, S., Fergusson, W.D., Whetton, A.D., Moreira-Leite, F., Pepper, S.D., Miller, C., Saunders, E.K., White, D.J., Will, A.M., Eden, T., et al. (2007). Amplification and translocation of 3q26 with overexpression of EVI1 in Fanconi anemia-derived childhood acute myeloid leukemia with biallelic FANCD1/BRCA2 disruption. Genes. Chromosomes Cancer *46*, 359–372. 10.1002/gcc.20417.

59. Malbert-Colas, L., Ponnuswamy, A., Olivares-Illana, V., Tournillon, A.-S., Naski, N., and Fåhraeus, R. (2014). HDMX folds the nascent p53 mRNA following activation by the ATM kinase. Mol. Cell *54*, 500–511. 10.1016/j.molcel.2014.02.035.

60. Layer, R.M., Chiang, C., Quinlan, A.R., and Hall, I.M. (2014). LUMPY: a probabilistic framework for structural variant discovery. Genome Biol. *15*, R84. 10.1186/gb-2014-15-6-r84.

61. Chiang, C., Layer, R.M., Faust, G.G., Lindberg, M.R., Rose, D.B., Garrison, E.P., Marth, G.T., Quinlan, A.R., and Hall, I.M. (2015). SpeedSeq: ultra-fast personal genome analysis and interpretation. Nat. Methods *12*, 966–968. 10.1038/nmeth.3505.

62. Zeitouni, B., Boeva, V., Janoueix-Lerosey, I., Loeillet, S., Legoix-né, P., Nicolas, A., Delattre, O., and Barillot, E. (2010). SVDetect: a tool to identify genomic structural variations from paired-end and mate-pair sequencing data. Bioinforma. Oxf. Engl. *26*, 1895–1896. 10.1093/bioinformatics/btq293.

63. Rausch, T., Zichner, T., Schlattl, A., Stütz, A.M., Benes, V., and Korbel, J.O. (2012). DELLY: structural variant discovery by integrated paired-end and split-read analysis. Bioinforma. Oxf. Engl. *28*, i333–i339. 10.1093/bioinformatics/bts378.

64. Schröder, J., Hsu, A., Boyle, S.E., Macintyre, G., Cmero, M., Tothill, R.W., Johnstone, R.W., Shackleton, M., and Papenfuss, A.T. (2014). Socrates: identification of genomic rearrangements in tumour genomes by re-aligning soft clipped reads. Bioinforma. Oxf. Engl. *30*, 1064–1072. 10.1093/bioinformatics/btt767.

65. Boeva, V., Popova, T., Bleakley, K., Chiche, P., Cappo, J., Schleiermacher, G., Janoueix-Lerosey, I., Delattre, O., and Barillot, E. (2012). Control-FREEC: a tool for assessing copy number and allelic content using next-generation sequencing data. Bioinforma. Oxf. Engl. *28*, 423–425. 10.1093/bioinformatics/btr670.

66. Soulier, J. (2011). Fanconi anemia. Hematol. Am. Soc. Hematol. Educ. Program *2011*, 492–497. 10.1182/asheducation-2011.1.492.

67. Pinto, F.O., Leblanc, T., Chamousset, D., Le Roux, G., Brethon, B., Cassinat, B., Larghero, J., de Villartay, J.-P., Stoppa-Lyonnet, D., Baruchel, A., et al. (2009). Diagnosis of Fanconi anemia in patients with bone marrow failure. Haematologica *94*, 487–495. 10.3324/haematol.13592.

68. Soulier, J., Leblanc, T., Larghero, J., Dastot, H., Shimamura, A., Guardiola, P., Esperou, H., Ferry, C., Jubert, C., Feugeas, J.-P., et al. (2005). Detection of somatic mosaicism and classification of Fanconi anemia patients by analysis of the FA/BRCA pathway. Blood *105*, 1329–1336. 10.1182/blood-2004-05-1852.

69. Arber, D.A., Orazi, A., Hasserjian, R., Thiele, J., Borowitz, M.J., Le Beau, M.M., Bloomfield, C.D., Cazzola, M., and Vardiman, J.W. (2016). The 2016 revision to the World Health Organization classification of myeloid neoplasms and acute leukemia. Blood *127*, 2391–2405. 10.1182/blood-2016-03-643544.

70. Cioc, A.M., Wagner, J.E., MacMillan, M.L., DeFor, T., and Hirsch, B. (2010). Diagnosis of myelodysplastic syndrome among a cohort of 119 patients with fanconi anemia: morphologic and cytogenetic characteristics. Am. J. Clin. Pathol. *133*, 92–100. 10.1309/AJCP7W9VMJENZOVG.

71. Sébert, M., Passet, M., Raimbault, A., Rahmé, R., Raffoux, E., Sicre de Fontbrune, F., Cerrano, M., Quentin, S., Vasquez, N., Da Costa, M., et al. (2019). Germline DDX41 mutations define a significant entity within adult MDS/AML patients. Blood *134*, 1441–1444. 10.1182/blood.2019000909.

72. Chalmers, Z.R., Connelly, C.F., Fabrizio, D., Gay, L., Ali, S.M., Ennis, R., Schrock, A., Campbell, B., Shlien, A., Chmielecki, J., et al. (2017). Analysis of 100,000 human cancer genomes reveals the landscape of tumor mutational burden. Genome Med. *9*, 34. 10.1186/s13073-017-0424-2.

73. Zhao, E.Y., Shen, Y., Pleasance, E., Kasaian, K., Leelakumari, S., Jones, M., Bose, P., Ch'ng, C., Reisle, C., Eirew, P., et al. (2017). Homologous Recombination Deficiency and Platinum-Based Therapy Outcomes in Advanced Breast Cancer. Clin. Cancer Res. Off. J. Am. Assoc. Cancer Res. *23*, 7521–7530. 10.1158/1078-0432.CCR-17-1941.

74. Anders, S., Pyl, P.T., and Huber, W. (2015). HTSeq--a Python framework to work with high-throughput sequencing data. Bioinforma. Oxf. Engl. *31*, 166–169. 10.1093/bioinformatics/btu638.

75. Makuch, R.W., and Simon, R.M. (1980). Sample size considerations for non-randomized comparative studies. J. Chronic Dis. *33*, 175–181. 10.1016/0021-9681(80)90017-x.

76. H Turner, D Firth. Bradley-Terry models in R: the BradleyTerry2 package-Journal of Statistical Software, 2012,48(9),1-21.

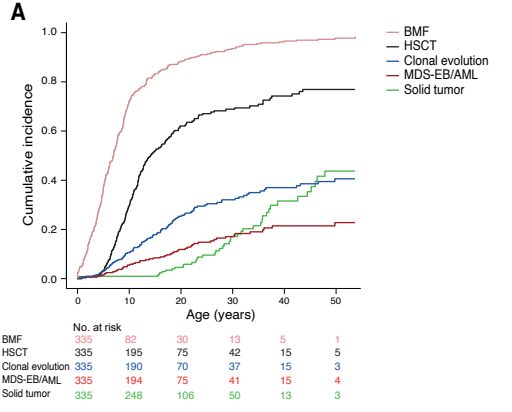
A
Cumulative incidence
1.0
0.8
0.6
0.4
0.2
0.0
0
10
20
30
40
50
Age (years)
BMF
HSCT
Clonal evolution
MDS-EB/AML
Solid tumor
No. at risk
BMF 335 82 30 13 5 1
HSCT 335 195 75 42 15 5
Clonal evolution 335 190 70 37 15 3
MDS-EB/AML 335 194 75 41 15 4
Solid tumor 335 248 106 50 13 3
B
Overall survival
1.00
0.75
0.50
0.25
0.00
0 6 12 18 24 30 36 42 48 54 60 63
Age (years)
No. at risk
335 308 216 134 81 57 30 15 8 5 4 1
C
Overall survival
1.0
0.8
0.6
0.4
0.2
0.0
Time-dependent covariate
Non-clonal (see legend)
Clonal evolution
p=0.003
(HR=1.53, 95%CI, 1.10-2.13)
0 10 20 30 40 50 60
Time (years)
No. at risk
237 169 69 35 12 2 1
98 80 39 22 5 4 3

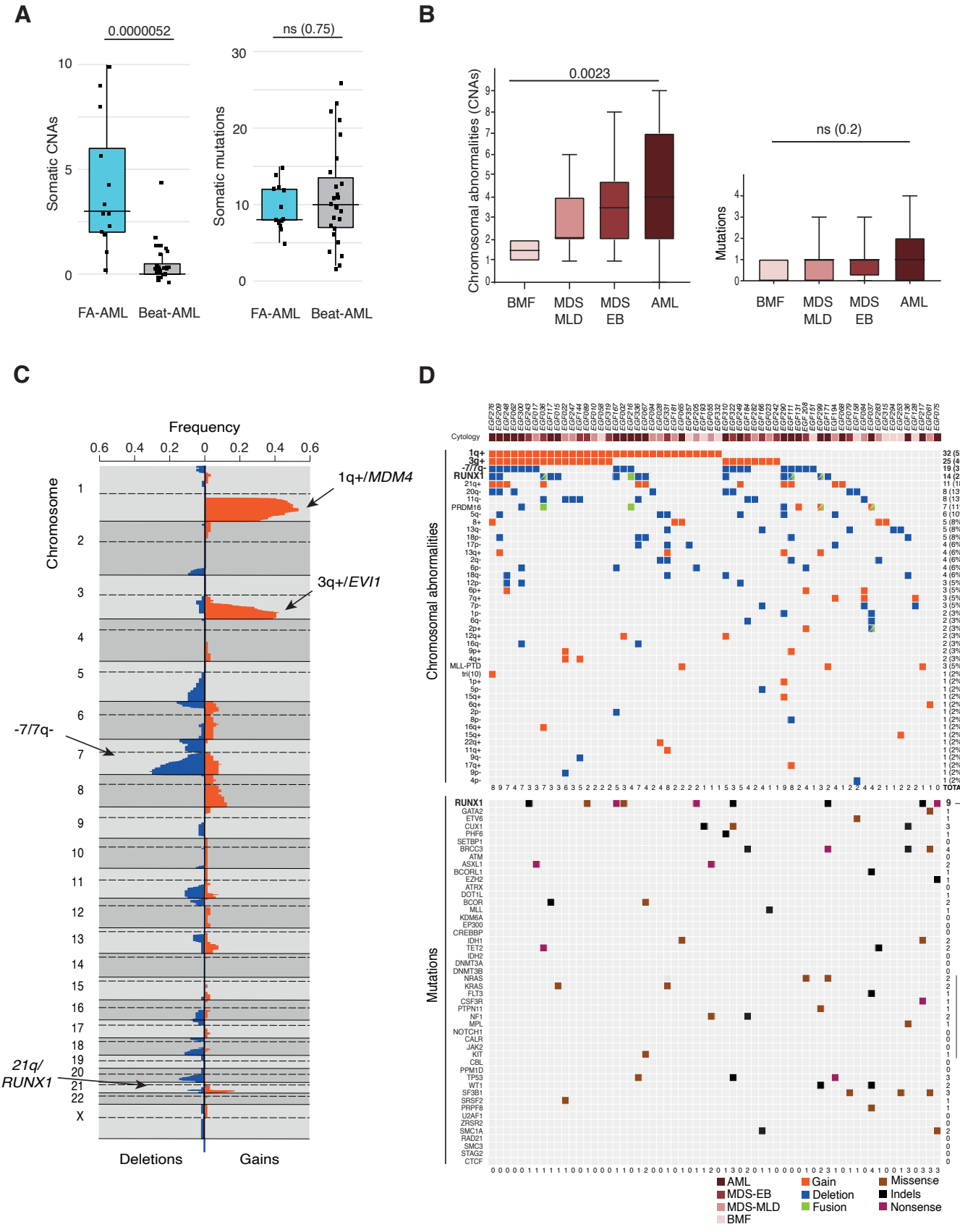
A
0.0000052
ns (0.75)
Somatic CNAs
Somatic mutations
FA-AML
Beat-AML
B
0.0023
ns (0.2)
Chromosomal abnormalities (CNAs)
Mutations
BMF
MDS MLD
MDS EB
AML
C
Frequency
Chromosome
1q+/MDM4
3q+/EVI1
-7/7q-
21q/ RUNX1
Deletions
Gains
D
Cytology
Chromosomal abnormalities
Mutations
Signal transduction
RUNX1
GATA2
ETV6
CUX1
PHF6
SETBP1
BRCC3
ATM
ASXL1
BCORL1
EZH2
ATRX
DOT1L
BCOR
MLL
KDM6A
EP300
CREBBP
IDH1
TET2
IDH2
DNMT3A
DNMT3B
NRAS
KRAS
FLT3
CSF3R
PTPN11
NF1
MPL
NOTCH1
CALR
JAK2
KIT
CBL
PPM1D
TP53
WT1
SF3B1
SRSF2
PRPF8
U2AF1
ZRSR2
SMC1A
RAD21
SMC3
STAG2
CTCF
AML
MDS-EB
MDS-MLD
BMF
Gain
Deletion
Fusion
Missense
Indels
Nonsense

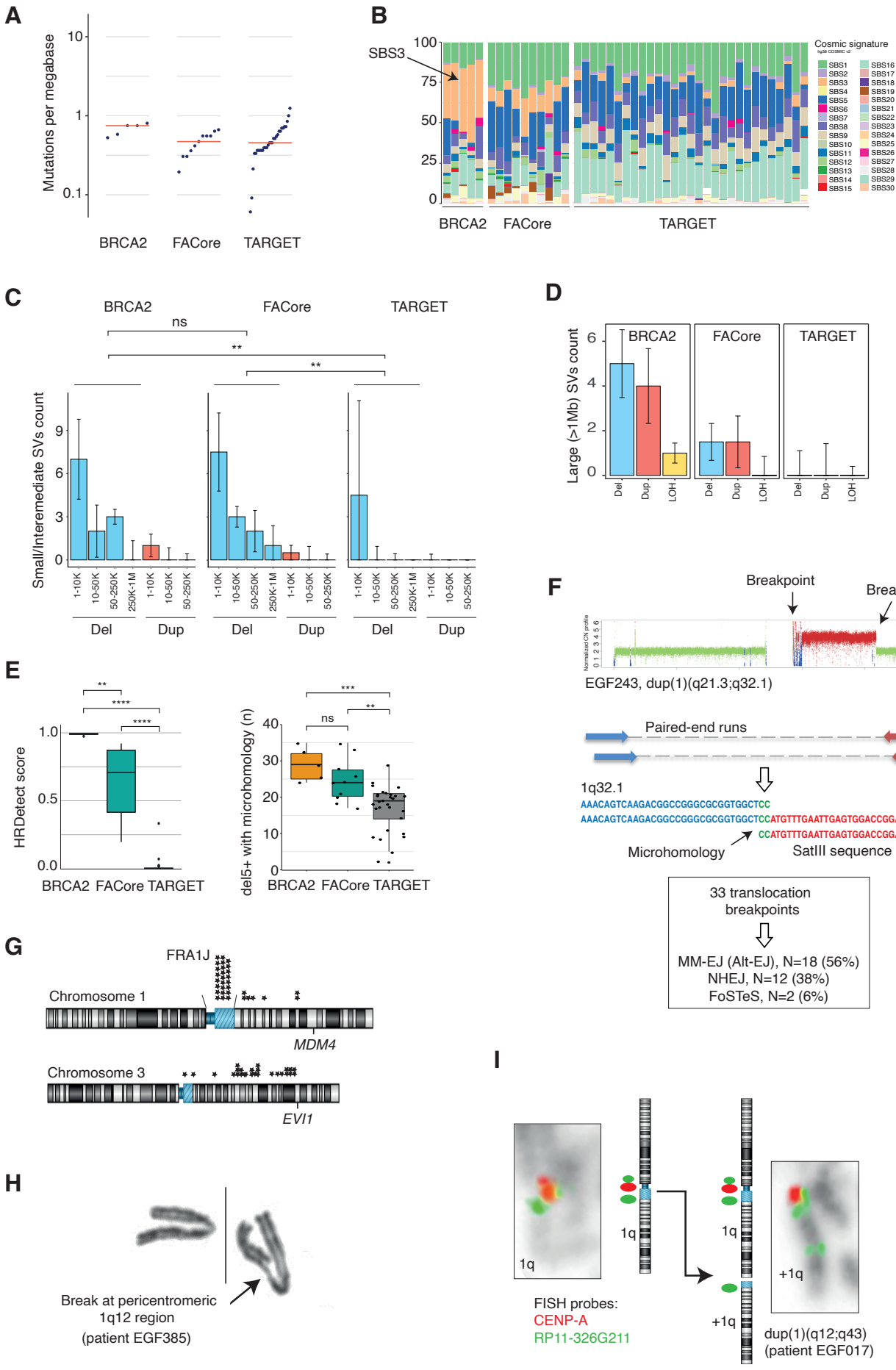
A
Mutations per megabase
10
1
0.1
BRCA2
FACore
TARGET
B
SBS3
100
75
50
25
0
BRCA2
FACore
TARGET
Cosmic signature
SBS1
SBS2
SBS3
SBS4
SBS5
SBS6
SBS7
SBS8
SBS9
SBS10
SBS11
SBS12
SBS13
SBS14
SBS15
SBS16
SBS17
SBS18
SBS19
SBS20
SBS21
SBS22
SBS23
SBS24
SBS25
SBS26
SBS27
SBS28
SBS29
SBS30
C
BRCA2
FACore
TARGET
ns
**
**
Small/Interemediate SVs count
9
6
3
0
1-10K
10-50K
50-250K
250K-1M
Del
Dup
D
Large (>1Mb) SVs count
6
4
2
0
BRCA2
FACore
TARGET
Del
Dup
LOH
E
HRDetect score
1.0
0.5
0.0
**
****
****
BRCA2 FACore TARGET
del5+ with microhomology (n)
40
30
20
10
0
***
ns
**
BRCA2 FACore TARGET
F
Breakpoint
Breakpoint
EGF243, dup(1)(q21.3;q32.1)
Paired-end runs
1q32.1
AAACAGTCAAGACGGCCGGGCGCGGTGGCTCC
AAACAGTCAAGACGGCCGGGCGCGGTGGCTCCATGTTTGAATTGAGTGGACCGGAAAATAAT
CCATGTTTGAATTGAGTGGACCGGAAAATAAT
Microhomology
SatIII sequence
33 translocation breakpoints
MM-EJ (Alt-EJ), N=18 (56%)
NHEJ, N=12 (38%)
FoSTeS, N=2 (6%)
G
FRA1J
Chromosome 1
MDM4
Chromosome 3
EVI1
H
Break at pericentromeric 1q12 region
(patient EGF385)
I
1q
1q
1q
+1q
+1q
FISH probes:
CENP-A
RP11-326G211
dup(1)(q12;q43)
(patient EGF017)

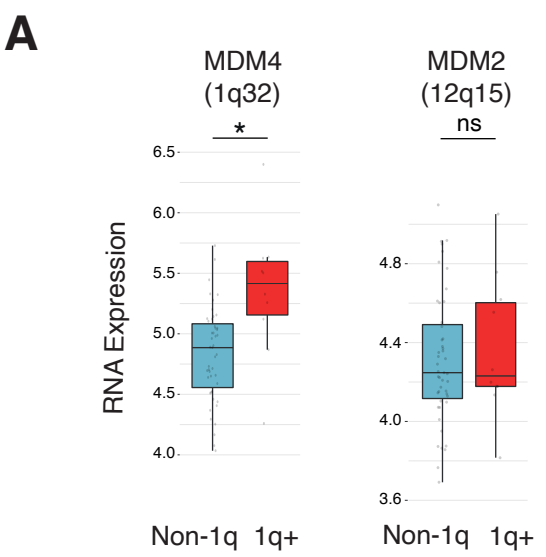
A
MDM4
(1q32)
*
MDM2
(12q15)
ns
RNA Expression
6.5
6.0
5.5
5.0
4.5
4.0
4.8
4.4
4.0
3.6
Non-1q 1q+
Non-1q 1q+

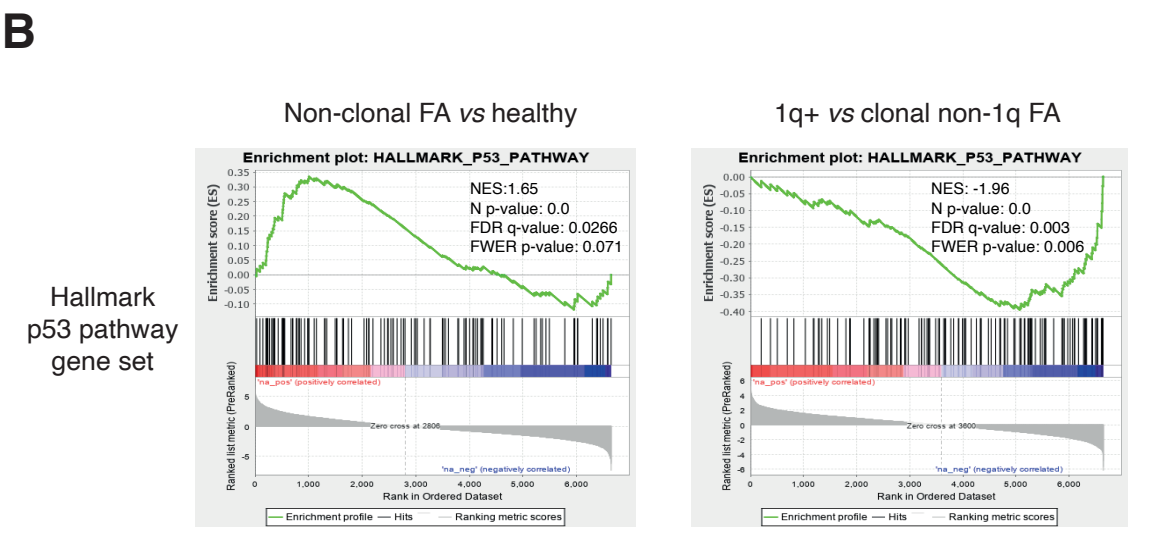
B
Non-clonal FA vs healthy
1q+ vs clonal non-1q FA
Hallmark
p53 pathway
gene set
Enrichment plot: HALLMARK_P53_PATHWAY
NES:1.65
N p-value: 0.0
FDR q-value: 0.0266
FWER p-value: 0.071
Enrichment score (ES)
'na_pos' (positively correlated)
Zero cross at 2806
'na_neg' (negatively correlated)
Ranked list metric (PreRanked)
Rank in Ordered Dataset
Enrichment profile
Hits
Ranking metric scores
Enrichment plot: HALLMARK_P53_PATHWAY
NES: -1.96
N p-value: 0.0
FDR q-value: 0.003
FWER p-value: 0.006
Enrichment score (ES)
'na_pos' (positively correlated)
Zero cross at 3600
'na_neg' (negatively correlated)
Ranked list metric (PreRanked)
Rank in Ordered Dataset
Enrichment profile
Hits
Ranking metric scores

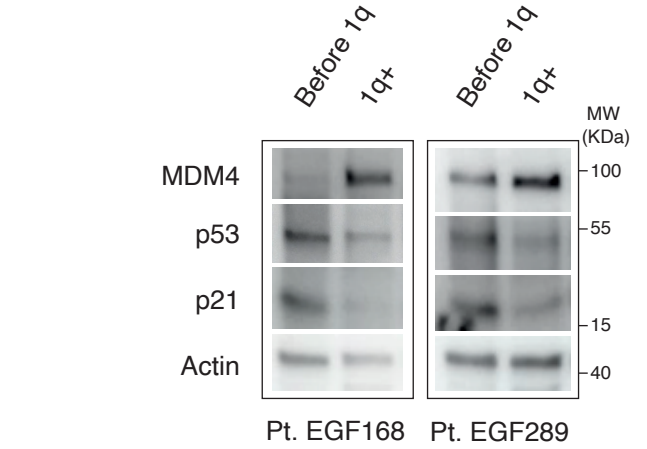
C
Before 1q+
1q+
Before 1q+
1q+
MW
(KDa)
MDM4
p53
p21
Actin
100
55
15
40
Pt. EGF168
Pt. EGF289

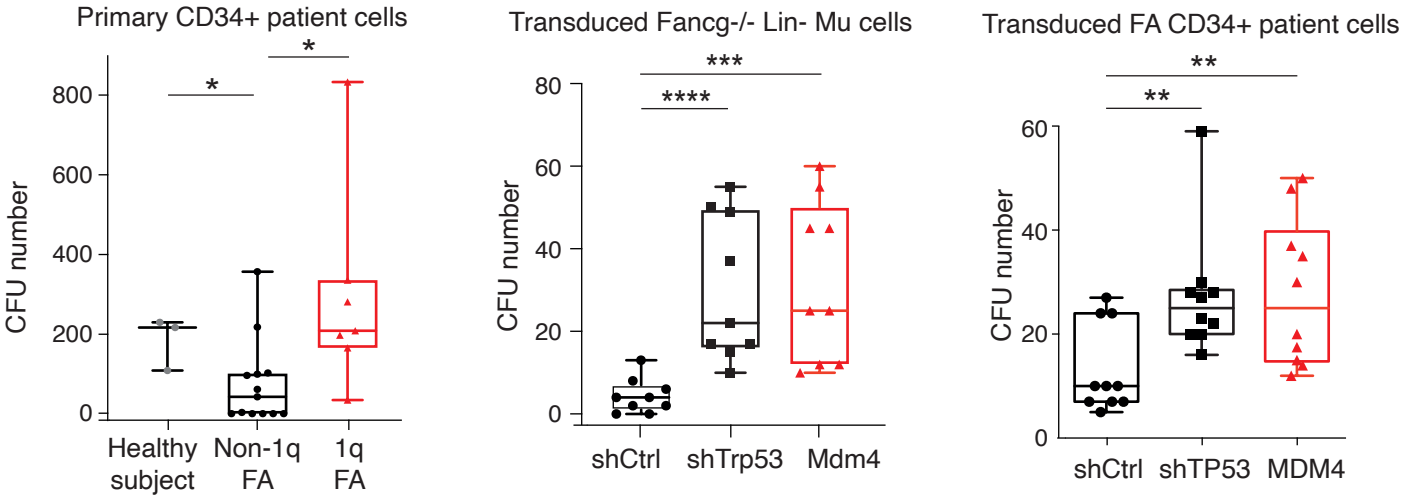
D
Primary CD34+ patient cells
CFU number
800
600
400
200
0
*
*
Healthy subject
Non-1q FA
1q FA
E
Transduced Fancg-/- Lin- Mu cells
CFU number
80
60
40
20
0
***
****
shCtrl
shTrp53
Mdm4
F
Transduced FA CD34+ patient cells
CFU number
60
40
20
0
**
**
shCtrl
shTP53
MDM4

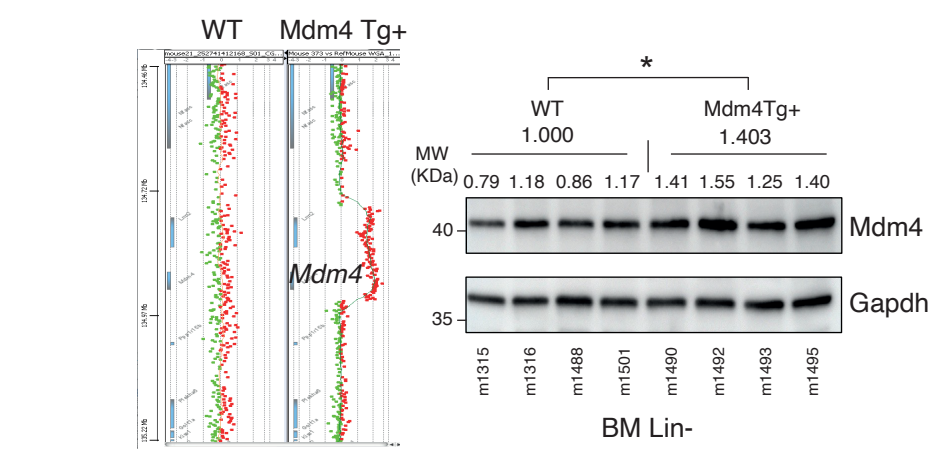
G
WT
Mdm4 Tg+
Mdm4
MW
(KDa)
WT
1.000
Mdm4Tg+
1.403
0.79 1.18 0.86 1.17 1.41 1.55 1.25 1.40
40
Mdm4
35
Gapdh
m1315
m1316
m1488
m1501
m1490
m1492
m1493
m1495
BM Lin-

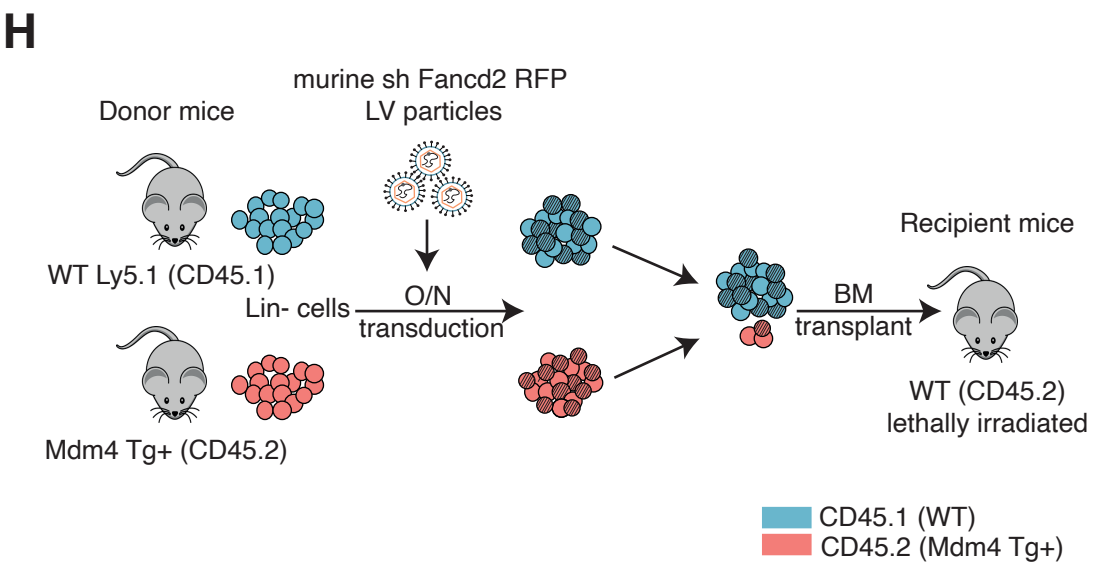
H
murine sh Fancd2 RFP
LV particles
Donor mice
WT Ly5.1 (CD45.1)
Lin- cells
O/N
transduction
Mdm4 Tg+ (CD45.2)
BM
transplant
Recipient mice
WT (CD45.2)
lethally irradiated
CD45.1 (WT)
CD45.2 (Mdm4 Tg+)

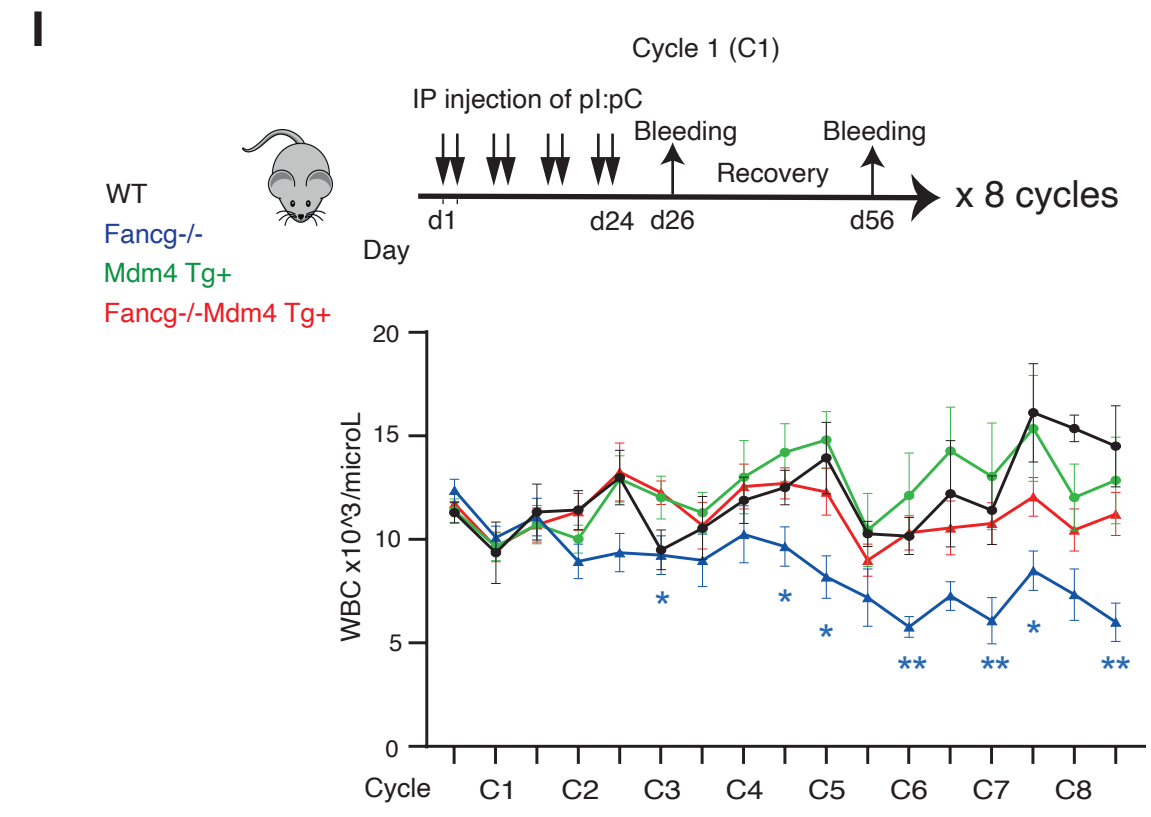
I
Cycle 1 (C1)
IP injection of pI:pC
Bleeding
Bleeding
Recovery
x 8 cycles
WT
Fancg-/-
Mdm4 Tg+
Fancg-/-Mdm4 Tg+
d1
d24
d26
d56
Day
WBC x10^3/microL
20
15
10
5
0
Cycle
C1
C2
C3
C4
C5
C6
C7
C8

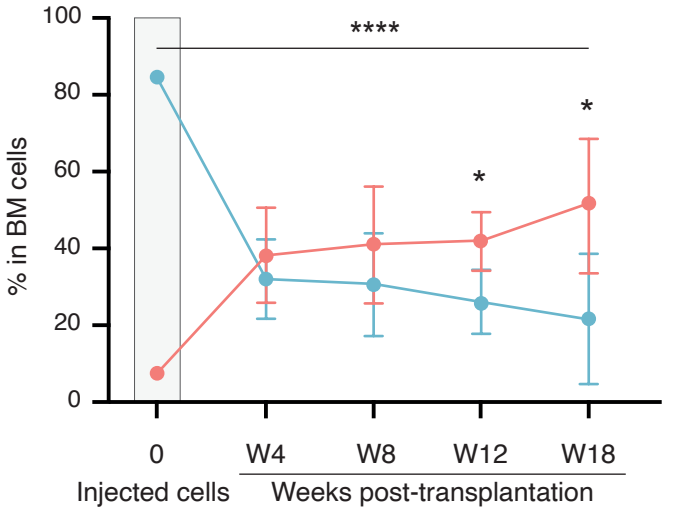
****
*
*
100
80
60
40
20
0
% in BM cells
0
W4
W8
W12
W18
Injected cells
Weeks post-transplantation

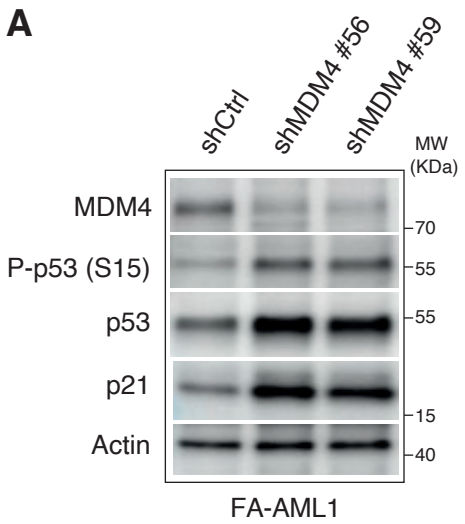
A
shCtrl
shMDM4 #56
shMDM4 #59
MW (KDa)
MDM4
P-p53 (S15)
p53
p21
Actin
70
55
55
15
40
FA-AML1

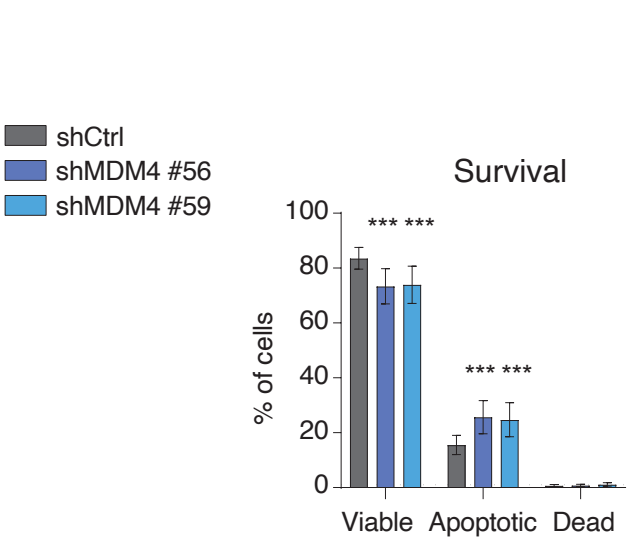
B
shCtrl
shMDM4 #56
shMDM4 #59
Survival
% of cells
100
80
60
40
20
0
*** ***
*** ***
Viable
Apoptotic
Dead

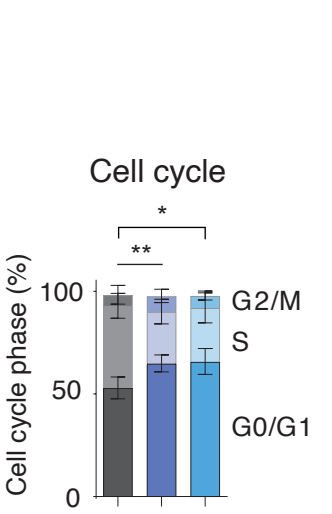
C
Cell cycle
Cell cycle phase (%)
100
50
0
*
**
G2/M
S
G0/G1

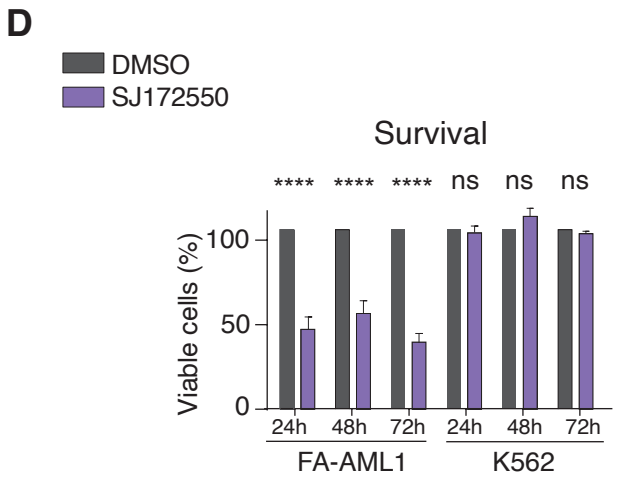
D
DMSO
SJ172550
Survival
Viable cells (%)
100
50
0
**** **** **** ns ns ns
24h 48h 72h 24h 48h 72h
FA-AML1
K562

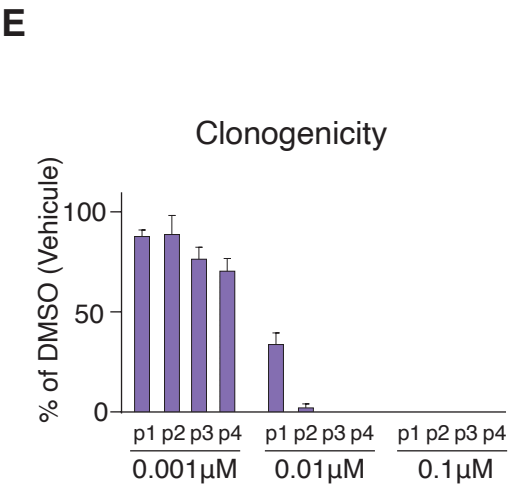
E
Clonogenicity
% of DMSO (Vehicule)
100
50
0
p1 p2 p3 p4
p1 p2 p3 p4
p1 p2 p3 p4
0.001µM
0.01µM
0.1µM

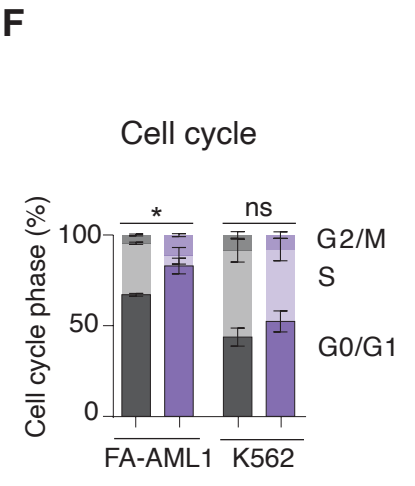
F
Cell cycle
Cell cycle phase (%)
100
50
0
*
ns
G2/M
S
G0/G1
FA-AML1
K562

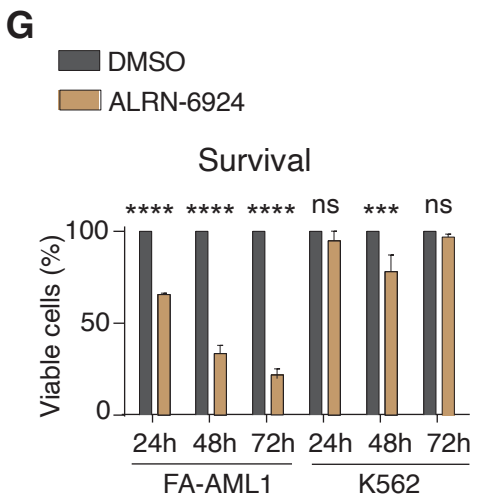
G
DMSO
ALRN-6924
Survival
Viable cells (%)
100
50
0
**** **** **** ns *** ns
24h 48h 72h 24h 48h 72h
FA-AML1
K562

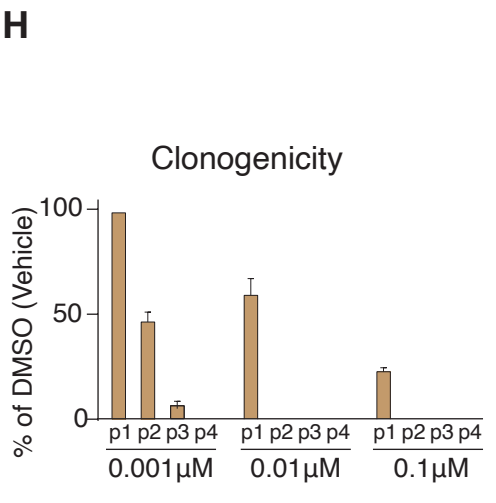
H
Clonogenicity
% of DMSO (Vehicle)
100
50
0
p1 p2 p3 p4
p1 p2 p3 p4
p1 p2 p3 p4
0.001µM
0.01µM
0.1µM

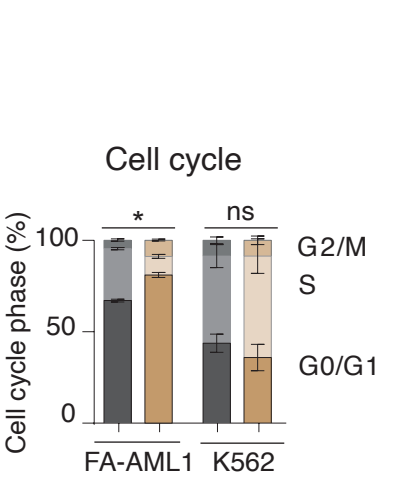
I
Cell cycle
Cell cycle phase (%)
100
50
0
*
ns
G2/M
S
G0/G1
FA-AML1
K562

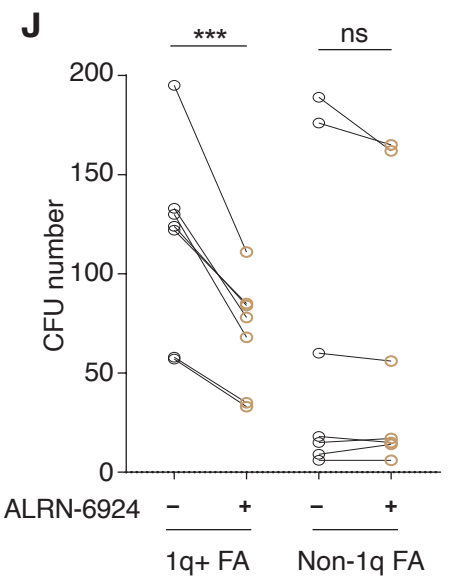
J
CFU number
200
150
100
50
0
*** ns
ALRN-6924
– + – +
1q+ FA
Non-1q FA

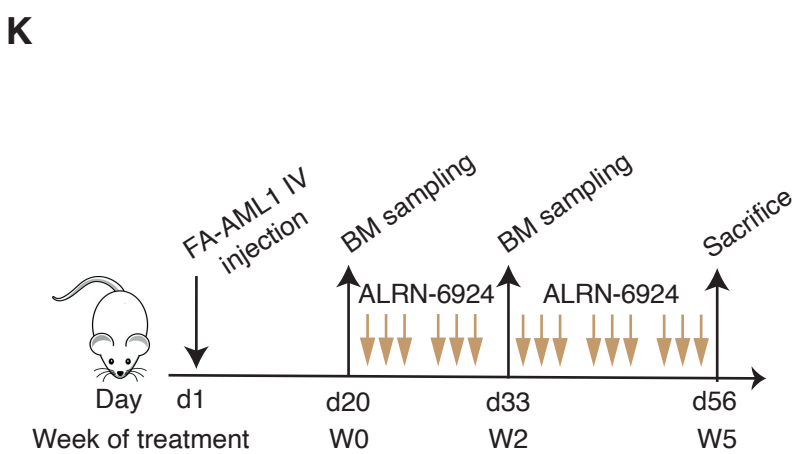
K
FA-AML1 IV injection
BM sampling
BM sampling
Sacrifice
ALRN-6924
ALRN-6924
Day
d1
d20
d33
d56
Week of treatment
W0
W2
W5

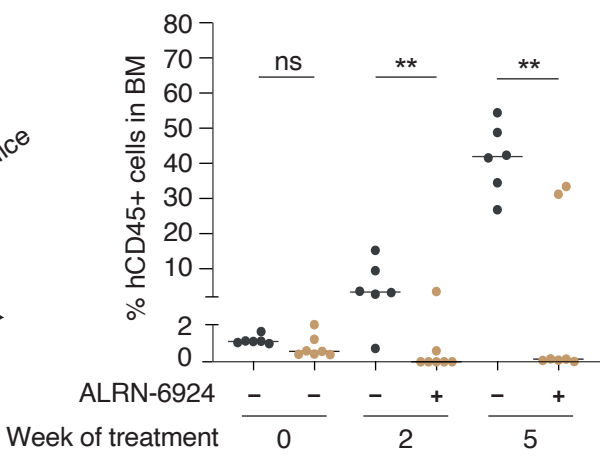
% hCD45+ cells in BM
80
70
60
50
40
30
20
10
2
0
ns ** **
ALRN-6924
– – – + – +
Week of treatment
0
2
5

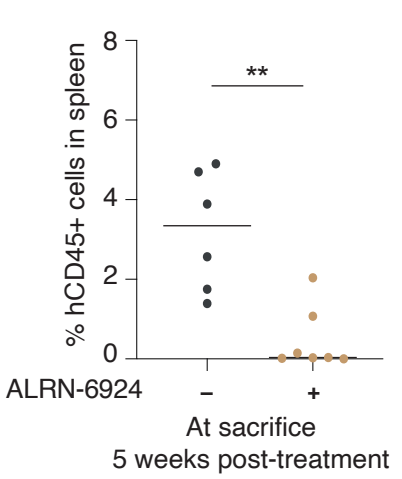
% hCD45+ cells in spleen
8
6
4
2
0
**
ALRN-6924
– +
At sacrifice
5 weeks post-treatment

Figure 6

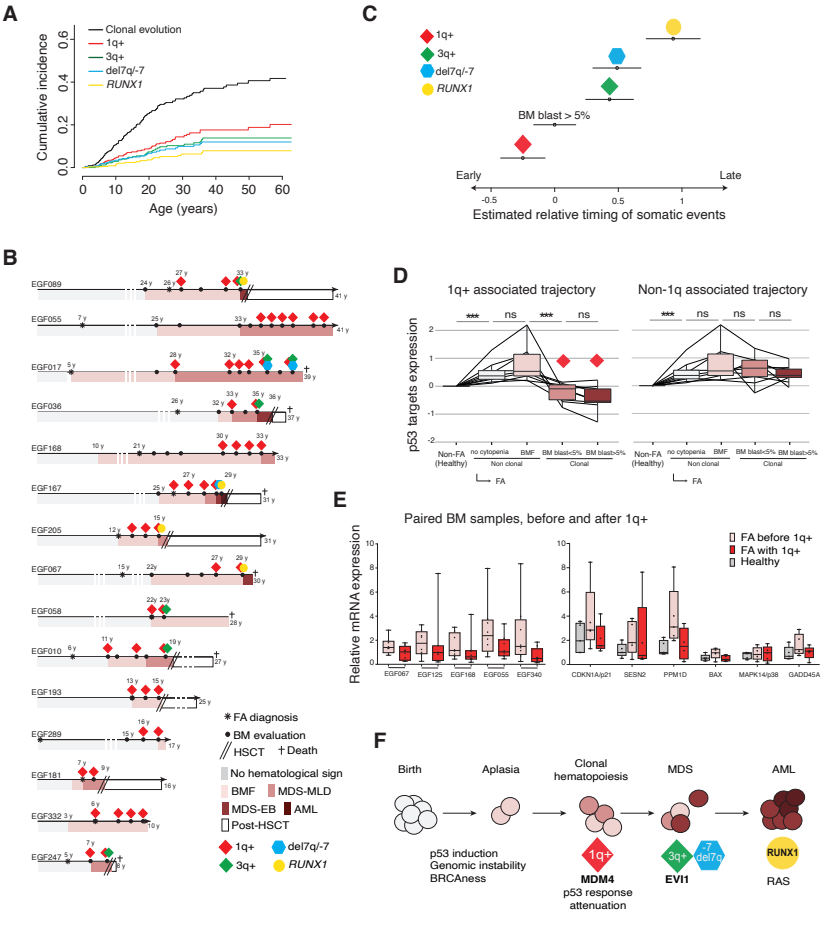
A
Clonal evolution
1q+
3q+
del7q/-7
RUNX1
Cumulative incidence
0.0
0.2
0.4
0.6
0
10
20
30
40
50
60
Age (years)
C
1q+
3q+
del7q/-7
RUNX1
BM blast > 5%
Early
Late
-0.5
0
0.5
1
Estimated relative timing of somatic events
B
EGF089
EGF055
EGF017
EGF036
EGF168
EGF167
EGF205
EGF067
EGF058
EGF010
EGF193
EGF289
EGF181
EGF332
EGF247
FA diagnosis
BM evaluation
HSCT
Death
No hematological sign
BMF
MDS-MLD
MDS-EB
AML
Post-HSCT
1q+
3q+
del7q/-7
RUNX1
D
1q+ associated trajectory
Non-1q associated trajectory
p53 targets expression
***
ns
Non-FA (Healthy)
no cytopenia
BMF
BM blast<5%
BM blast>5%
Non clonal
Clonal
FA
E
Paired BM samples, before and after 1q+
Relative mRNA expression
FA before 1q+
FA with 1q+
Healthy
EGF067
EGF125
EGF168
EGF055
EGF340
CDKN1A/p21
SESN2
PPM1D
BAX
MAPK14/p38
GADD45A
F
Birth
Aplasia
Clonal hematopoiesis
MDS
AML
p53 induction
Genomic instability
BRCAness
1q+
MDM4
p53 response attenuation
3q+
-7
del7q
EVI1
RUNX1
RAS

Figure 7

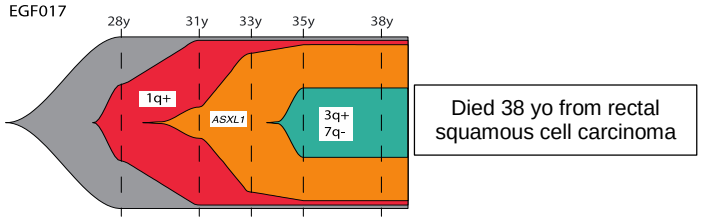

Age	Revised karyotype	FISH 1q (MDM4)	FISH 3q (EVI1)	FISH 7q (KMT2E and MET)	aCGH	NGS
28y	46,XY,dup(1)(q12;q43)[7]/46,XY[9]	3 signals	2 signals	2 signals	-	-
31y	-	-	-	-	1q+ (95%)	ASXL1 (VAF:9%)
33y	46,XY,dup(1)(q12;q43)[20]	3 signals	2 signals	2 signals	1q+ (95%)	ASXL1 (VAF:41%)
35y	46,XY,dup(1)(q12;q43)[7]/46,idem,del(7)(q31)[13]	3 signals	3 signals	1 signal	1q+ (95%), 3q+(40%), del7q (40%)	ASXL1 (VAF:44%)
38y	46,XY,dup(1)(q12;q43)[8]/46,idem,del(7)(q31)[9]/46,XY,der(1;5)(q10;q35)[3]	3 signals	3 signals	1 signal	-	-

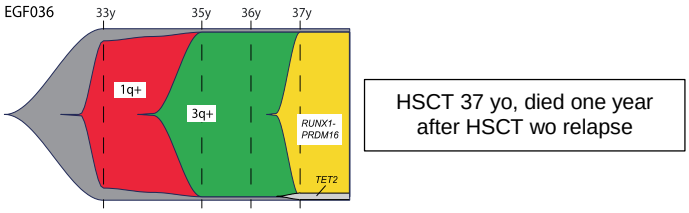

Age	Revised karyotype	FISH 1q (MDM4)	FISH 3q (EVI1)	FISH 7q (KMT2E and MET)	aCGH	NGS
33y	46,XX,der(16)t(1;16)(q21;q32)[17]/46,XX[3]	3 signals	2 signals	2 signals	-	Normal
35y	46,XX,der(2)t(2;3)(q22;q21),der(16)t(1;16)(q21;q32)[12]	3 signals	3 signals	2 signals	1q+ (95%), 3q+ (95%)	TET2 (VAF:3%)
36y	46,XX,der(2)t(2;3)(q22;q21),der(16)t(1;16)(q21;q32)[19]	3 signals	3 signals	2 signals	-	-
37y	46,XX,der(1)t(1;21)(p36;q22).ish(PRDM16+,RUNX1+),der(2)t(2;3)(q22;q21),der(16)t(1;16)(q21;q32)[20	3 signals	3 signals	2 signals	-	-

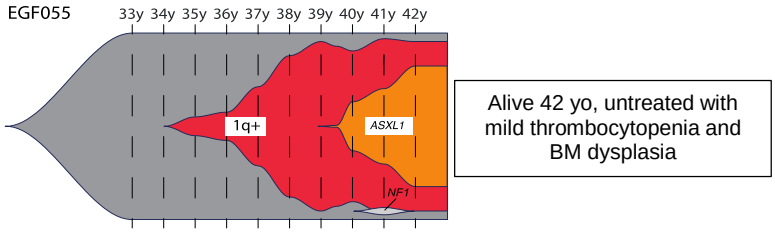

Age	Revised karyotype	FISH 1q (MDM4)	FISH 3q (EVI1)	FISH 7q (KMT2E and MET)	aCGH	NGS
33y	46,XX[6]	2 signals	2 signals	2 signals	-	-
34y	46,XX[15]	2 signals	2 signals	2 signals	-	-
35y	46,XX,der(13)t(1;13)(q11;p11)[4]/46,XX[26]	3 signals	2 signals	2 signals	Normal	-
36y	46,XX,der(13)t(1;13)(q11;p11)[6]/46,XX[25]	3 signals	2 signals	2 signals	Normal	-
37y	46,XX,der(13)t(1;13)(q11;p11)[5]/46,XX[7]	3 signals	2 signals	2 signals	1q+ (50%)	Normal
38y	46,XX,der(13)t(1;13)(q11;p11)[3]/46,XX[4]	3 signals	2 signals	2 signals	-	-
39y	46,XX,der(13)t(1;13)(q11;p11)[2]	3 signals	2 signals	2 signals	-	-
40y	46,XX,der(13)t(1;13)(q11;p11)[16]/46,XX[4]	3 signals	2 signals	2 signals	-	ASXL1 (VAF:13%)
41y	46,XX,der(13)t(1;13)(q11;p11)[13]/46,XX[1]	3 signals	2 signals	2 signals	-	ASXL1 (VAF:13%), NF1 (VAF:2%)
42y	46,XX,der(13)t(1;13)(q11;p11)[10]/46,XX[1]	3 signals	2 signals	2 signals	-	ASXL1 (VAF: 32%)

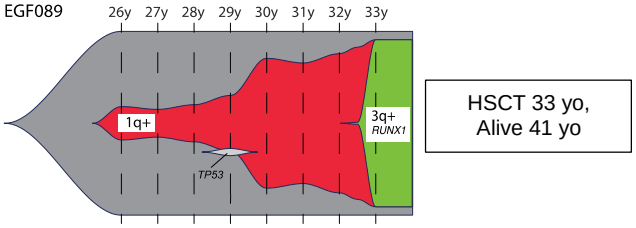

Age	Revised karyotype	FISH 1q (MDM4)	FISH 3q (EVI1)	FISH 7q (KMT2E and MET)	aCGH	NGS
26y	46,XY,dup(1)(q12;q41)[3]/46,XY[17]	3 signals	2 signals	2 signals	-	-
27y	45,X,-Y[9]/46,XY,dup(1)(q12;q41)[2]/46,XY[13]	3 signals	2 signals	2 signals	1q+ (15%)	-
28y	46,XY,dup(1)(q12;q41)[3]/46,XY[16]	3 signals	2 signals	2 signals	-	-
29y	45,X,-Y[6]/46,XY,dup(1)(q12;q41)[5]/46,XY[8]	3 signals	2 signals	2 signals	1q+ (30%)	TP53 (VAF:4%)
30y	46,XY,dup(1)(q12;q41)[14]/46,XY[8]	3 signals	2 signals	2 signals	-	-
31y	46,XY,dup(1)(q12;q41)[13]/45,X,-Y[2]/46,XY[10]	3 signals	2 signals	2 signals	-	-
32y	46,XY,dup(1)(q12;q41)[15]/45,X,-Y[1]/46,XY[4]	3 signals	2 signals	2 signals	-	-
33y	46,XY,dup(1)(q12;q41), der(10)t(3;10)(q26;q26)[10]/46,XY[7]	3 signals	3 signals	2 signals	1q+ (90%), 3q+ (90%)	RUNX1 (VAF:42%)

Fanconi anemia bone marrow progression